

Dynamic Glycosylation Governs the Vertebrate COPII Protein Trafficking Pathway

Nathan J. Cox,^{†,‡,§} Gokhan Unlu,[§] Brittany J. Bisnett,[†] Thomas R. Meister,[†] Brett M. Condon,[†] Peter M. Luo,[†] Timothy J. Smith,[†] Michael Hanna,^{||} Abhishek Chhetri,[†] Erik J. Soderblom,[⊥] Anjon Audhya,^{||} Ela W. Knapik,[§] and Michael Boyce^{*,†,‡,§}

[†]Department of Biochemistry and [‡]Pharmacological Sciences Training Program, Duke University School of Medicine, Durham, North Carolina 27710, United States

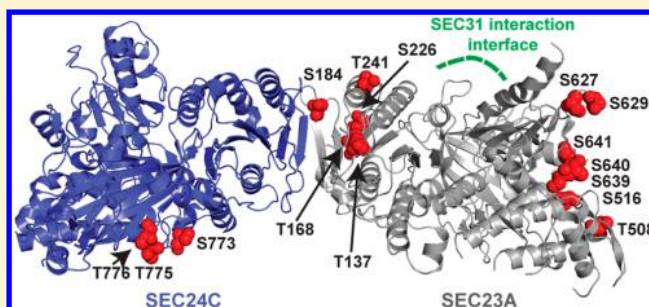
[§]Departments of Medicine and Cell and Developmental Biology, Vanderbilt University Medical Center, Nashville, Tennessee 37232, United States

^{||}Department of Biomolecular Chemistry, University of Wisconsin—Madison School of Medicine and Public Health, Madison, Wisconsin 53706, United States

[⊥]Duke Proteomics and Metabolomics Core Facility, Center for Genomic and Computational Biology, Duke University, Durham, North Carolina 27710, United States

S Supporting Information

ABSTRACT: The COPII coat complex, which mediates secretory cargo trafficking from the endoplasmic reticulum, is a key control point for subcellular protein targeting. Because misdirected proteins cannot function, protein sorting by COPII is critical for establishing and maintaining normal cell and tissue homeostasis. Indeed, mutations in COPII genes cause a range of human pathologies, including cranio-lenticulo-sutural dysplasia (CLSD), which is characterized by collagen trafficking defects, craniofacial abnormalities, and skeletal dysmorphism. Detailed knowledge of the COPII pathway is required to understand its role in normal cell physiology and to devise new treatments for disorders in which it is disrupted. However, little is known about how vertebrates dynamically regulate COPII activity in response to developmental, metabolic, or pathological cues. Several COPII proteins are modified by O-linked β -N-acetylglucosamine (O-GlcNAc), a dynamic form of intracellular protein glycosylation, but the biochemical and functional effects of these modifications remain unclear. Here, we use a combination of chemical, biochemical, cellular, and genetic approaches to demonstrate that site-specific O-GlcNAcylation of COPII proteins mediates their protein–protein interactions and modulates cargo secretion. In particular, we show that individual O-GlcNAcylation sites of SEC23A, an essential COPII component, are required for its function in human cells and vertebrate development, because mutation of these sites impairs SEC23A-dependent *in vivo* collagen trafficking and skeletogenesis in a zebrafish model of CLSD. Our results indicate that O-GlcNAc is a conserved and critical regulatory modification in the vertebrate COPII-dependent trafficking pathway.



One-third of eukaryotic proteins pass through the secretory pathway for targeting to specific locations, including the endoplasmic reticulum (ER), Golgi, plasma membrane, and extracellular space.^{1–3} As a result, properly regulated protein secretion is required for cellular and organismal physiology. In particular, coat protein complex II (COPII), which mediates anterograde trafficking from the ER, is a key component of the early secretory pathway.^{4–9} The formation of a COPII transport carrier begins when the cytosolic GTPase SAR1 binds GTP and inserts into the ER membrane, a process facilitated by the ER-anchored guanine nucleotide exchange factor SEC12.^{4–6} Active SAR1-GTP recruits SEC23/SEC24 heterodimers, which effect the loading of cargo into the nascent carriers via protein–protein interactions among SEC24 and client or adaptor proteins.^{4–6,10,11} Then, SEC13/SEC31 heterotetramers assemble over the SAR1/SEC23/SEC24

prebudding complex, forming the outer layer of a polyhedral cage that promotes membrane curvature and scission, resulting in a mature COPII transport carrier.^{4–6}

The COPII pathway is required for protein sorting and cell viability in a wide range of organisms,^{4–6} and genetic defects in COPII components cause a variety of human diseases, including cranio-lenticulo-sutural dysplasia (CLSD), hematological disorders, a subtype of osteogenesis imperfecta (OI), and multiple hereditary spastic paraplegias.^{4–6,12–25} Interestingly, the molecular etiology of these diseases can often be attributed to aberrant

Special Issue: Future of Biochemistry

Received: September 1, 2017

Revised: October 30, 2017

Published: November 21, 2017

trafficking of particular COPII client cargoes. For example, mutations in *SEC23A* (which cause CLSD) and *SEC24D* (which cause a subtype of OI) both disrupt collagen trafficking, leading to chondrocyte dysfunction, impaired skeletogenesis, craniofacial disease, and bone deformities.^{15,18,21–23,26–30}

Despite this broad pathophysiological importance, major aspects of COPII trafficking remain poorly understood. For instance, while the fundamental steps of COPII assembly are relatively well characterized, little is known about how vertebrate cells modulate this activity in response to developmental cues, fluctuating signals, metabolic demands, or stress.^{4–6} The COPII cargo load changes dramatically in both normal (e.g., stimulated B cells or differentiating pancreatic β islets) and pathological (e.g., nutrient, redox, or proteostasis stress) contexts,^{31–37} but the mechanisms through which the COPII machinery adjusts to these changes are largely unclear.

Post-translational modifications (PTMs) represent one likely general mode of COPII pathway regulation. For example, phosphorylation^{38–44} and ubiquitination^{45–47} of individual COPII proteins govern particular aspects of vesicular trafficking. Recently, we⁴⁸ and others^{49–52} have also shown that multiple COPII components, including SEC23, SEC24, and SEC31, are modified by O-linked β -N-acetylglucosamine (O-GlcNAc) in mammalian cells. O-GlcNAc is a major intracellular PTM, reversibly decorating serine and threonine side chains of thousands of nuclear, cytoplasmic, and mitochondrial proteins, and is broadly conserved across animals, plants, and perhaps some fungi.^{53–56} In animals, O-GlcNAc is added by O-GlcNAc transferase (OGT) and removed by O-GlcNAcase (OGA), both ubiquitous nuclear/cytoplasmic enzymes.^{53–56} O-GlcNAc cycling controls myriad processes, including cell metabolism, cell cycle progression, and cell death,^{53–56} and is essential, as genetic ablation of OGT or OGA is lethal in mice.^{57,58} Because several core COPII proteins are O-GlcNAcylated,^{48–52} we reasoned that this intracellular glycosylation might regulate protein trafficking. Consistent with this notion, the level of SEC24 O-GlcNAcylation is high during interphase but low during mitosis, when COPII-dependent trafficking is suspended through an unknown mechanism,⁵⁰ suggesting that O-GlcNAc may dynamically control COPII function during cell cycle progression. However, the mechanistic and functional effects of O-GlcNAc on the COPII pathway have not been explored.

Here, we address the prevalence, biochemical effects, and physiological importance of O-GlcNAcylation in the COPII pathway. We show that O-GlcNAc is widespread in the COPII system and that site-specific glycosylation of key COPII proteins impacts protein secretion. Moreover, we use a chemical biology approach to demonstrate that dynamic O-GlcNAcylation mediates the protein–protein interactions of COPII components, identifying a new potential biochemical mechanism for cargo trafficking regulation by this PTM. Using a genome-engineered human cell model, we show that individual glycosylation sites of SEC23A, an essential COPII component, are required to traffic endogenous collagen. Finally, we demonstrate that mutation of specific O-GlcNAc sites impairs *in vivo* SEC23A-dependent collagen trafficking in a zebrafish model of CLSD. Together, our results establish O-GlcNAc as a conserved and prevalent regulatory modification in the vertebrate COPII pathway.

MATERIALS AND EXPERIMENTAL DETAILS

Chemical Synthesis. SSGlcNAc was synthesized as described previously⁵⁹ and was a gift of B. M. Swarts (Central Michigan University, Mt Pleasant, MI). Thiamet-G

and Ac₃GlcNDAz-1-P(Ac-SATE)₂ (“GlcNDAz”) were synthesized as described previously^{60,61} by the Duke Small Molecule Synthesis Facility. All other chemicals were purchased from Sigma-Aldrich unless otherwise indicated.

Western Blotting (WB). Samples were resolved on Tris-glycine sodium dodecyl sulfate–polyacrylamide gel electrophoresis (SDS–PAGE) gels and electroblotted onto a polyvinylidene fluoride (PVDF) membrane (88518, ThermoFisher) using standard methods.⁶² Membranes were blocked with Tris-buffered saline with 0.1% Tween (TBST) with 5% bovine serum albumin (BSA). All antibody dilutions were prepared in TBST with 5% BSA. Membranes were incubated with primary antibodies overnight at 4 °C, washed three times in TBST, incubated with secondary antibodies for 1 h at room temperature, washed three times in TBST, and developed via enhanced chemiluminescence (ECL) according to the manufacturer’s instructions (WesternBright ECL, Advanta). The following primary antibodies were used: rabbit anti-SEC23A (8162, Cell Signaling Technology, 1:2000), rabbit anti-SEC23A serum (gift of D. Ginsburg, University of Michigan, Ann Arbor, MI, 1:2000), rabbit anti-SEC23B serum (gift of D. Ginsburg, 1:2000), rabbit anti-SEC24C (8531, Cell Signaling Technology, 1:1000), rabbit anti-SEC24D (9610, Cell Signaling Technology, 1:1000), rabbit anti-SEC24B (7427, Cell Signaling Technology, 1:1000), rabbit anti-SEC31A (A302–336A, Bethyl, 1:2000), rabbit anti-TFG (A302–343A, Bethyl, 1:4000), mouse monoclonal α -tubulin (T6074, Sigma-Aldrich, 1:100000), rabbit monoclonal GAPDH (14C10) (2188, Cell Signaling Technology, 1:4000), mouse monoclonal anti-c-myc (9E10) (various vendors), mouse monoclonal anti-O-GlcNAc antibody 9D1 (MA1–039, ThermoFisher, 1:1000), mouse monoclonal anti-O-GlcNAc antibody RL2 (SC-59624, Santa Cruz Biotechnology, 1:500), and rabbit anti-TRAP α (gift of C. Nicchitta, Duke University, 1:8000). The following secondary antibodies were used: goat anti-mouse IgG [1030-05, horseradish peroxidase (HRP)-conjugated, SouthernBiotech, 1:10000] and goat anti-rabbit IgG (4030-05, HRP-conjugated, SouthernBiotech, 1:10000).

Cell Culture. 293T, HeLa, HeLa/UAP1(F383G), 293T/UAP1(F383G), COS7(tsVSVG-eGFP), and SW1353 (including all engineered derivative lines) cells were cultured in Dulbecco’s modified Eagle’s medium containing 10% fetal bovine serum, 100 units/mL penicillin, and 100 μ g/mL streptomycin in 5% CO₂ at 37 °C. Transduced cell lines were also supplemented with puromycin during regular passaging at the following concentrations: 1.5 μ g/mL for HeLa/UAP1(F383G) and 2 μ g/mL for 293T/UAP1(F383G) and COS7(tsVSVG-eGFP).

Mammalian Expression Vectors. pSin-EF2-UAP1(F383G) was a gift from J. Kohler (The University of Texas Southwestern Medical Center, Dallas, TX).⁶⁰ pmTurquoise2-Golgi was a gift from D. Gadella (Addgene plasmid no. 36205). mCherry-ER-3 was a gift from M. Davidson (Addgene plasmid no. 55041). The pMSCV tsVSVG-eGFP was generated by cutting tsVSVG-eGFP from the parent vector (pEGFP-VSVG, Addgene, plasmid no. 11912) with BglII and NotI and ligating it into pMSCV via standard methods.⁶² pcDNA4-SEC23A-myc-6xHis, pcDNA4-SEC31A-myc-6xHis, pcDNA3-myc-6xHis-SEC24C, p3xFLAG-SEC24C, pcDNA4-TFG-myc-6xHis, and p3xFLAG-TFG were generated by amplifying the open reading frames from their respective cDNA and ligating them into pcDNA4/myc-6xHis, pcDNA3-myc-6xHis, or p3xFLAG-CMV-10 using standard methods.⁶² Primers for site-directed mutagenesis were designed using QuikChange

Primer Design (<http://www.genomics.agilent.com/primerDesignProgram.jsp>). Mutagenesis reactions were performed using Phusion polymerase (M0530, New England Biolabs) essentially according to the manufacturer's instructions, but with an extra initial 30 s 98 °C denaturation step prior to the addition of polymerase. Mutagenesis reaction mixtures were digested with DpnI and transformed into One Shot TOP10 chemically competent *Escherichia coli* (C404010, ThermoFisher). The following primers and their reverse complements were used for site-directed mutagenesis: S97, 5'-CAGTTCAGATATACCAGCATAAGCAGGTGAAAAC-TGATTCCTTTGG-3'; S102, 5'-AGGCTGATTCAGTTCAGCTATACCAGCATAACTAGGTG-3'; S115A, CATATTCATGCTAGCAAATGAGGTAAGTTTTCAGCAGGCT; S116A, CACGAGAATACATATTCATTCATCTTCCATGCAAGCATCAACCACATAGAGGAATATC; T168A, CCATTCTCCAAAAGCAATAAGTCCAACCAAGCTGTAGGT; S184, 5'-CTCTGAAGACATAGCTTTTTGCAATGCTTCACATCCAAGTTC-3'; S226A, GTAAGAATCTGTGGCAGGAGGTGGCTGCTGTAC; T241A, GAGTTCCTCCAGAAGATCTGCGAGATTCATGTCTATTTTCT; T508A, TGTTTTGGATTTGAGCTTGAGCATCTGCCAGTTCC; S516A, TGCCTCCTGGTCAAAGCTGCAGCAATGTTTTGGA; S627, 5'-CCTATCCTGTATGCGTATGCTTTAGTGGACCACCAG-3'; S629, 5'-CTCTGGTGGTCCAGCAAAAGAATACGCATACAGGATAGGC-3'; S639, 5'-GCAAGAATGCTACTGCGATCAAGAAGAACCGGCTCTGGT-3'; S640, 5'-ACGATCTGCAAGAATGCTAGCGCTATCAAGAAGAACCGGC-3'; S641, 5'-GAATACGATCTGCAAGAATGGCACTGCTATCAAGAAGAACCG-3'.

Stable Cell Line Creation. UAP1(F383G) and tsVSVG-eGFP retro- and lentiviruses were generated in 293T-17 cells using calcium phosphate transfection and standard methods as described previously.⁴⁸ Medium containing virus was filtered through prewetted 0.45 μ m PVDF syringe filters, and 1 mL of the viral supernatant was added directly to 10 cm plates of 50% confluent cells. HeLa/UAP1(F383G) and 293T/UAP1(F383G) cells were selected using 1.5 and 2 μ g/mL puromycin, respectively.⁶⁰ COS7(tsVSVG-eGFP) cells were selected using 2 μ g/mL puromycin until cells exhibited green ER fluorescence.

Immunoprecipitation and Tandem Affinity Purification. Cells transfected with myc-6xHis- or 3xFLAG-tagged proteins were lysed in immunoprecipitation (IP) lysis buffer [1% Triton X-100, 0.1% SDS, 150 mM NaCl, 1 mM EDTA, and 20 mM Tris-HCl (pH 7.4)] supplemented with protease inhibitor cocktail (P8340, Sigma), with 50 μ M UDP and 5 μ M PUGNAc (17151, Cayman Chemicals) to inhibit endogenous OGT and hexosaminidases, respectively. Lysates were probe-sonicated, cleared by centrifugation, and quantified by the BCA protein assay (23225, ThermoFisher) according to the manufacturer's instructions. IPs were performed on 2–10 mg of total protein (for WB) or 50–100 mg of total protein (for MS analysis). Cleared lysates were adjusted to a final total protein concentration of ~2–5 mg/mL using IP lysis buffer supplemented with protease inhibitor, UDP and PUGNAc, and 2 μ g of mouse monoclonal anti-c-myc (9E10) (sc-40, Santa Cruz Biotechnology) per milligram of total protein was added and the mixture rotated overnight at 4 °C; 50 μ L of washed protein A/G UltraLink Resin (53133, ThermoFisher) was added to the lysate and the mixture rotated at room temperature for 1 h. Beads were washed three times with 1 mL of

IP lysis buffer and then eluted. For IPs, elution was performed with IP lysis buffer and 2 \times SDS-PAGE loading buffer [5 \times SDS-PAGE loading buffer consisted of 250 mM Tris (pH 6.8), 10% SDS, 30% glycerol, 5% β -mercaptoethanol, and 0.02% bromophenol blue] and heating at 95 °C for 5 min. Eluents were then analyzed by SDS-PAGE and WB. For tandem affinity purification, beads were eluted twice in 500 μ L using Ni-NTA wash buffer (8 M urea, 300 mM NaCl, 1% Triton X-100, and 5 mM imidazole) with rotation. The two 500 μ L elutions were pooled, and 50 μ L of washed 6xHisPur Ni-NTA resin (88223, ThermoFisher) was added to the eluate and the mixture rotated for 2 h at room temperature. The Ni-NTA resin was washed three times with 1 mL of Ni-NTA wash buffer. Final elution from the Ni-NTA was performed using 8 M urea with 250 mM imidazole.

Digitonin Fractionation. Cells were seeded such that they were ~80% confluent in a 10 cm plate on the day of harvest. Cells were washed with 10 mL of cold PBS and incubated on ice for 10 min. PBS was removed from the plate, and 1 mL of permeabilization buffer [110 mM KOAc, 25 mM HEPES (pH 7.2), 2.5 mM Mg(OAc)₂, 1 mM EGTA, 0.015% digitonin, 1 mM dithiothreitol (DTT), and protease inhibitor cocktail] was added, taking care to not dislodge the cells, and incubated on ice for 5 min. Soluble material was collected from the plate into a new chilled 1.5 mL centrifuge tube and retained as the cytoplasmic fraction. The remaining cells were washed gently with 5 mL of wash buffer [110 mM KOAc, 25 mM HEPES (pH 7.2), 2.5 mM Mg(OAc)₂, 1 mM EGTA, 0.004% digitonin, and 1 mM DTT]. After being washed, the cells were incubated on ice in IP lysis buffer supplemented with protease inhibitor cocktail for 5 min and then scraped and moved into a chilled 1.5 mL centrifuge tube to obtain the membrane fraction. Both fractions were probe-sonicated and cleared by centrifugation. Equal volumes from each fraction were precipitated with methanol and chloroform to concentrate. Fractions were analyzed by SDS-PAGE and WB.

Densitometry. Western blot band densitometry readings were performed on scanned blot images using the gel analyzer tool within the Fiji software package.⁶³ Raw densitometry values were used to calculate cytoplasmic:membrane ratios for each protein within each experimental replicate.

tsVSVG-eGFP Imaging. Two days prior to imaging, 200000 COS7(tsVSVG-eGFP) cells were plated onto 35 mm glass-bottom dishes (P35GCol-1.5-14-C, MatTek) in phenol red-free Dulbecco's modified Eagle's medium containing 10% fetal bovine serum, 10 mM HEPES (pH 7.4), 100 units/mL penicillin, and 100 μ g/mL streptomycin in 5% CO₂. Sixteen hours prior to imaging, cells were shifted to 40 °C and 5% CO₂; 8 h prior to imaging, cells were treated with either vehicle (DMSO) or 25 μ M Thiamet-G. Cells were then shifted to the permissive temperature (32 °C and 5% CO₂), and images were collected every 10 s for 20 min. Imaging was performed on a Zeiss LSM 780 inverted confocal microscope, using 40 \times /1.4 NA Oil-Plan Apochromat DIC, (UV) VIS-IR (420762-9900), Zen 2011 software (Duke Light Microscopy Core Facility).

Transfections. Cells plated at ~50% confluence [or ~20% confluence, for GlcNDAz labeling experiments (see below)] were transfected the following day; 750 μ L of prewarmed OPTI-MEM (11058021, ThermoFisher) was placed in 1.5 mL tubes with 30 μ L of TransIT-293 transfection reagent (Mirus), vortexed briefly, and incubated for 15 min at room temperature. After incubation, 10 μ g of plasmid DNA was added to a 1.5 mL tube, vortexed briefly, and incubated for 15 min at room

temperature. After the final incubation, the transfection mixture was added dropwise to the cells. For GlcNDAz cross-linking experiments (see below), GlcNDAz was added 24 h after transfection. For other experiments, cells were harvested 24–48 h post-transfection.

HRP Secretion Assay. 293T cells were plated on 10 cm dishes, cultured until they were 80% confluent, and transfected with 20 μg of ssHRP construct using *TransIT-LT1* transfect reagent (Mirus) as described above. Twenty-four hours post-transfection (and 4 h before collection of the supernatant), cells were pretreated with 5SGlcNAc or vehicle only. After 4 h, medium was aspirated, and cells were gently washed with PBS. Fresh medium containing either 5SGlcNAc or vehicle was re-added. At each time point, 50 μL of medium was removed from the plate and stored at 4 °C until analysis was performed. To quantify ssHRP secretion, 10 μL of medium from each time point was added to a clear-bottom white 96-well plate with 50 μL of a premixed ECL solution (WesternBright ECL, Advansta), and luminescence was measured on a Spectramax M5e plate reader (Molecular Devices) with an integration time of 500 ms.

Cell Viability Assay. 293T cells were transfected with the ssHRP plasmid as described above. After 24 h, cells were trypsinized and 25000 cells in 100 μL of DMEM were seeded into clear-bottom 96-well plates and treated as described above. After an additional 24 h, the MTS assay was performed according to the manufacturer's protocol (Promega, CellTiter 96 AQueous Proliferation Assay kit, G3581). Reported values are an average of technical triplicate reads minus the absorbance from control wells containing medium only.

GlcNDAz Cross-Linking. Cells stably expressing UAP1-(F383G) were plated at ~50% confluence without puromycin. If transfection was being performed first, cells were plated at ~20% confluence. The next day, 100 μM GlcNDAz⁶⁰ or vehicle was added to the cells. Medium was changed, and fresh GlcNDAz was added every 24 h. After GlcNDAz treatment for 48–72 h, plates were placed on ice, lids were removed, and medium was replaced with ice-cold PBS. Cells were irradiated with a 365 nm ultraviolet (UV) lamp (Blak-Ray XX-20BLB UV Bench Lamp, model 95-0045-04) for 20 min to induce cross-linking. Cells were collected by being scraped into PBS and centrifugation, lysed in IP lysis buffer, and analyzed by the BCA assay, SDS-PAGE, and WB.

Mass Spectrometry (MS) O-GlcNAc Site Mapping. Eight hours prior to being harvested, 293T-17 cells transfected with myc-6xHis-tagged COPII components were treated with 25 μM Thiamet-G and 4 mM glucosamine. Tandem affinity-purified SEC23A, SEC24C, or SEC31A was separated by SDS-PAGE, visualized by colloidal Coomassie blue, excised, and subjected to a standardized in-gel trypsin digestion (<http://www.genome.duke.edu/cores/teomics/sample-preparation/documents/In-gelDigestionProtocolrevised.pdf>). Extracted peptides were lyophilized to dryness and resuspended in 20 μL of 0.2% formic acid and 2% acetonitrile. Each sample was subjected to chromatographic separation on a Waters NanoAquity UPLC instrument equipped with a 1.7 μm BEH130 C₁₈ 75 μm (inside diameter) \times 250 mm reversed-phase column. The mobile phase consisted of (A) 0.1% formic acid in water and (B) 0.1% formic acid in acetonitrile. Following a 2 μL injection, peptides were trapped for 3 min on a 5 μm Symmetry C₁₈ 180 μm (inside diameter) \times 20 mm column at a rate of 5 $\mu\text{L}/\text{min}$ in 99.9% A. The analytical column was then switched in-line, and a linear elution gradient

from 5 to 40% B was performed over 90 min at a rate of 400 nL/min. The analytical column was connected to a fused silica PicoTip emitter (New Objective, Cambridge, MA) with a 10 μm tip orifice and coupled to a QExactive Plus mass spectrometer (ThermoFisher) through an electrospray interface operating in a data-dependent mode of acquisition. The instrument was set to acquire a precursor MS scan from m/z 375 to 1675 with MS/MS spectra acquired for the 10 most abundant precursor ions. For all experiments, high-energy collisional dissociation (HCD) energy settings were 27 V, and a 120 s dynamic exclusion was employed for previously fragmented precursor ions.

Raw LC-MS/MS data files were processed in Proteome Discoverer (ThermoFisher) and then submitted to independent Mascot searches (Matrix Science) against a SwissProt database (human taxonomy) containing both forward and reverse entries of each protein (20322 forward entries). Search tolerances were 5 ppm for precursor ions and 0.02 Da for product ions using semi-trypsin specificity with up to two missed cleavages. Carbamidomethylation (+57.0214 Da on Cys) was set as a fixed modification, whereas oxidation (+15.9949 Da on Met), deamidation (+0.98 Da on Asn/Gln), O-GlcNAc (+203.0793 Da on Ser/Thr), and phosphorylation (+79.9663 Da on Ser/Thr/Tyr) were considered dynamic mass modifications. All searched spectra were imported into Scaffold (version 4.7, Proteome Software), and scoring thresholds were set to achieve a peptide false discovery rate of <1% using the PeptideProphet algorithm. Localized O-GlcNAcylated residues were manually verified on the basis of annotated mass spectra generated within Mascot. In the SEC23A sample, peptides assigned by Mascot to SEC23B were assumed to be the cognate peptides in SEC23A, because SEC23A was purified to homogeneity.

Generation of SEC23A^{-/-} SW1353 Cells. LentiCas9 virus was obtained from the Duke Functional Genomics Facility. SW1353 cells were plated in six-well plates to be ~50% confluent at the time of infection. Prior to infection, medium was replaced with fresh medium containing 4 $\mu\text{g}/\text{mL}$ Polybrene, and 50 μL of LentiCas9 virus was added dropwise to the cells. Plates were then centrifuged at 700g for 30 min and incubated at 37 °C and 5% CO₂ overnight. The following morning, medium was replaced, and cells were allowed to recover for 48 h. After recovery, cells were selected using 3 $\mu\text{g}/\text{mL}$ blasticidin and passaged until a control, uninfected plate contained no living cells. These cells were dubbed SW1353/Cas9.

A single-guide RNA (sgRNA) sequence spanning the start codon of the human SEC23A locus was designed and validated via the Surveyor assay⁶⁴ by the Duke Functional Genomics Facility (5'-TTCCAAATAGGTTGTCATTG-3'). An sgRNA targeting AAVS1, commonly used as a control and deemed the "safe harbor" virus (SHV) locus,⁶⁵ was used as a control. Lentiviruses encoding the SEC23A sgRNA and the AAVS1 sgRNA were obtained from the Duke Functional Genomics Facility.

SW1353/Cas9 cells were plated in six-well plates to be ~50% confluent at the time of infection. Prior to infection, medium was replaced with fresh medium containing 4 $\mu\text{g}/\text{mL}$ Polybrene, and 50 μL of SEC23A or AAVS1 sgRNA lentivirus was added dropwise to the cells. Plates were then centrifuged at 700g for 30 min and incubated at 37 °C and 5% CO₂ overnight. The following morning, medium was replaced, and cells were allowed to recover for 48 h. After recovery, infected cells were selected using 0.25 $\mu\text{g}/\text{mL}$ puromycin and passaged until a control, uninfected plate contained no living cells. A decrease in

the level of SEC23A expression was verified on a mixed population level via WB.

Next, using serial dilution, single cells were plated in 96-well plates for both SEC23A and AAVS1 sgRNA-containing populations, and clones were allowed to recover and expand. Cells were transferred to larger plates under selective pressure of 3 $\mu\text{g}/\text{mL}$ blasticidin and 0.25 $\mu\text{g}/\text{mL}$ puromycin. A Western blot was used to verify loss of SEC23A expression. One SEC23A^{-/-} clone (SW23A-3) and one AAVS1 safe harbor control clone (SHV-23) were used in subsequent reconstitution experiments.

Generation of Stable SEC23A-Reconstituted SW23A-3 Cells.

SW23A-3 cells were plated to be ~30% confluent in six-well plates the following day. Then, medium was replaced prior to transfections; 150 μL of prewarmed OPTI-MEM was placed in 1.5 mL tubes with 9 μL of TransIT-LT1 transfection reagent (Mirus), vortexed briefly, and incubated for 15 min at room temperature. After incubation, 3 μg of plasmid DNA for either pcDNA4-myc-6xHis (empty vector), pcDNA4-GFP-myc-6xHis, or pcDNA4-SEC23A-myc-6xHis (wild type and serine to alanine point mutants) were added to a 1.5 mL tube, vortexed briefly, and incubated for 15 min at room temperature. After the final incubation, the transfection mixture was added dropwise to the cells. Cells recovered at 37 °C and 5% CO₂ for 48 h and then were selected using 200 $\mu\text{g}/\text{mL}$ Zeocin. Cells were passaged under selective pressure until a mock-transfected plate no longer contained living cells, the GFP-transfected control plate showed a majority of positive cells under fluorescent illumination, and other resistant colonies were expanding. Cell populations were also examined for stable transfectants using myc immunofluorescence.

SEC23B Knockdown via siRNA in SW1353. Glass coverslips were dipped in 100% ethanol, flame-sterilized, and placed in six-well plates with medium. Cells were plated to be ~15% the following day. The next morning, two reaction tubes per condition were prepared, both containing 125 μL of prewarmed OPTI-MEM; 100 pmol of a 1:1 mixture of SEC23B siRNA 1 and 2 was added to the first reaction tube (reaction 1) and incubated for 2 min. The same was done for control SEC23B scrambled siRNA 1 and 2. Next, 3 μL per 100 pmol of Lipofectamine RNAiMAX Transfection Reagent (Thermo Fisher) was added to the other tube containing 125 μL of prewarmed OPTI-MEM (reaction 2). Then, reaction 1 was added to reaction 2, flicked to mix, and incubated at room temperature for 20 min. During the incubation, fresh medium was added to the cells. After 20 min, the combined mixture was added dropwise to the cells. After being knocked down for 72 h, cells were used in IF experiments.

siRNA sequences targeting SEC23B have been described⁶⁶ and were ordered from Sigma-Aldrich as duplexes. Scrambled siRNAs were generated from parent sequences using Invivogen's siRNA Wizard scramble tool (<http://www.invivogen.com/sirnazard/scrambled.php>). Scrambled sequences were checked using NCBI BLAST to verify no significant homology in the human genome: SEC23B siRNA 1, 5'-CACGUUACAUCAAC-ACGGA[dT][dT]; SEC23B siRNA 2, 5'-CACUAUGAGAUGCUCUUGCUA[dT][dT]; SEC23B scrambled siRNA 1, 5'-GAAC-CCGCACGUAACUAU[dT][dT]; SEC23B scrambled siRNA 2, 5'-GCCAAUGCGUCUUGUAAAU[dT][dT].

Collagen Immunofluorescence Trafficking Assay. After SEC23B knockdown via siRNA, cells were treated with 50 $\mu\text{g}/\text{mL}$ ascorbate for 7 h. Then, cells were washed three times with PBS and fixed with 4% paraformaldehyde in PBS for

20 min. Following fixation, cells were washed three times with PBS and permeabilized using 0.1% Triton X-100 in PBS for 10 min. After permeabilization, cells were washed three times using PBS and then blocked using 0.1% BSA in PBS for 30 min. Following blocking, glass coverslips were transferred to microcentrifuge caps inside a humidified six-well plate. Primary antibody dilutions in 0.1% BSA were added to the coverslips and incubated overnight at 4 °C. The next day, coverslips were transferred back to their original six-well plate for washing and washed three times with PBS. Coverslips were again transferred to microcentrifuge caps inside a humidified six-well plate and incubated at room temperature for 1 h with appropriate Alexa Fluor secondary antibodies in 0.1% BSA. Coverslips were washed three times in PBS and transferred to glass slides with ProLong Diamond Antifade Mountant with DAPI (Thermo Fisher). Slides were cured at room temperature in a dark cabinet for at least 24 h before being imaged. The following primary antibodies were used: anti-myc (9E10, BioLegend, 626801, 1:500) and anti-collagen I antiserum (LF-68, a gift from L. Fisher, National Institute of Dental and Craniofacial Research, Bethesda, MD, 1:2000). The following secondary antibodies were used: goat anti-rabbit Alexa Fluor 488 (Thermo-Fisher, A-11008, 1:2000) and goat anti-mouse Alexa Fluor 594 (Thermo-Fisher, A-11005, 1:2000). At least 200 cells from each cell line were counted per biological replicate. Imaging was performed on a Zeiss LSM 780 inverted confocal microscope, using 40 \times /1.4 NA Oil-Plan Aplanochrom DIC, (UV) VIS-IR (420762-9900), Zen 2011 software (Duke Light Microscopy Core Facility).

General Immunofluorescence Staining. Cells were plated on glass coverslips and treated as indicated. After being treated, cells were fixed, permeabilized, stained, and mounted as described above. The following primary antibodies were used: protein disulfide isomerase (PDI) (C81H6, Cell Signaling Technology, 3501, 1:100), SEC16 (A300-648A, Bethyl, 1:500), and human procollagen type I C-peptide (QED Bioscience, 42024, 1:500). The following secondary antibodies were used: goat anti-rabbit Alexa Fluor 488 (Thermo-Fisher, A-11008, 1:2000), goat anti-mouse Alex Fluor 488 (Thermo-Fisher, A-11001, 1:2000), goat anti-mouse Alexa Fluor 594 (Thermo-Fisher, A-11005, 1:2000), and goat anti-rabbit 594 (Thermo-Fisher, A-11012).

Construction of Gateway Vectors for the Tol2kit System. The zebrafish *sec23a* coding sequence was amplified from the pCS2+ zSEC23a vector with primers containing attB1 (forward) and attB2 (reverse) recombineering sites. The fragment was purified and cloned into the pDONR221 vector using the Gateway BP clonase II enzyme mix. After successful cloning had been confirmed by sequencing, this plasmid was used as the middle entry vector for the Multistep Gateway Recombineering system, in combination with the pSE_1.7kbCol2a1a promoter,⁶⁷ p3E_v2a-EGFP (a gift from J. Gamse, Vanderbilt University), and pDestTol2pA2, and incubated with the Gateway LR clonase II enzyme mix overnight at room temperature. After transformation and colony screening, a destination vector was obtained that allows expression of the zebrafish *sec23a* coding sequence fused with a self-cleaving viral 2a peptide-tagged EGFP (v2a-EGFP) under the tissue-specific Col2a1a promoter. Four candidate SEC23A O-GlcNAc sites were sequentially mutated using the Q5 site-directed mutagenesis kit (New England Biolabs) with the following primers: 115–116F, TCCACAGTTTgcagct-ATTGAATATGTTGTC; 115–116R, AGTAGCTCAGCAGG-CTGG; 137F, TGTGGTGGACgCGTGCATGGA; 137R,

TACAGGAAGTTCAGGGGCATTTG; 168F, GGGCCTCA-TTgCATTTGGACGG; 168R, ACTAGGGCAGTAGGGGGC.

Zebrafish Microinjection. Zebrafish embryos at the one-cell stage were collected from *crusher*^{m299}/AB heterozygous crosses, injected with a combination of 50 pg of medaka transposase mRNA and 10 pg of *sec23a* destination vector DNA, and grown for 3 days in embryo medium.

Zebrafish Cryosectioning and Immunohistochemistry. Eighty hours postfertilization (hpf), embryos were fixed with 4% paraformaldehyde at 4 °C overnight and transferred to 30% sucrose in PBS. Embryos were embedded in Cryomatrix (ThermoFisher) and frozen at −80 °C for 15 min. Then, 14 μm thick sections were cut with a cryostat (Leica CM1900) and collected onto Fisherbrand Superfrost Plus slides. Slides were dried and rehydrated in PBS before staining. Following antigen retrieval (20 μg/mL proteinase K at room temperature for 5 min), embryos were permeabilized with 0.5% Triton X-100 in PBS for 10 min at room temperature. Samples were blocked (2% goat serum and 2 mg/mL BSA) for 30 min at room temperature, followed by overnight primary antibody incubation at 4 °C, using the 1:250 collagen II antibody (Rockland) and the 1:250 GFP antibody (Vanderbilt University Antibody and Protein Resource). Samples were incubated with secondary antibodies (rabbit AlexaFluor-555 and chicken AlexaFluor-488, Life Technologies) for 1 h and 1:4000 DAPI for 15 min at room temperature. Slides were mounted in ProlongGold (ThermoFisher).

Zebrafish Imaging and Quantification. Slides were imaged with Zeiss AxioImager.Z1. The percent collagen area in cytosol was calculated by the following formula: [collagen-positive intracellular area/(cytosol area − nucleus area marked by DAPI)] × 100. ImageJ⁶⁸ was used for intracellular area measurements.

RESULTS

Previous studies have indicated that COPII proteins are O-GlcNAcylated,^{48–52} but the biochemical and functional implications of these observations remain unclear. Indeed, O-GlcNAc sites have not been mapped systematically on any COPII protein, hindering subsequent biochemical and phenotypic experiments. As a first step toward understanding the role of O-GlcNAc cycling in anterograde trafficking, we analyzed the O-GlcNAcylation of three representative human COPII proteins, SEC23A, SEC24C, and SEC31A. We expressed and purified each protein to homogeneity from human cells and used mass spectrometry (MS) to map O-GlcNAcylated residues. Using high-stringency criteria, we detected at least 26, 11, and 10 O-GlcNAc modifications on SEC23A, SEC24C, and SEC31A, respectively, and manual inspection of the MS data permitted unambiguous assignment of many O-GlcNAc moieties to specific residues (Figure 1 and Figure S1). Interestingly, the glycosylation sites were not evenly distributed across each protein but rather were clustered in specific regions in all three cases. For example, five of the unambiguously assigned SEC23A O-GlcNAc sites (T137, T168, S184, S226, and S241) lie near its site of interaction with SEC24, as determined by prior structural studies,⁶⁹ whereas the others are distal to this interface (Figure 1B). In the case of SEC24C, the three definitively assigned glycosylation sites (S773, T775, and T776) reside in the relatively well-conserved β-sandwich domain. Finally, homology modeling based on structures of the yeast SEC31 ortholog suggests that all four assigned SEC31A glycosylation sites lie in the α-solenoid domain, which is thought to mediate protein–protein interactions and form a flexible hinge, permitting expansion of COPII carriers to

accommodate a range of cargo sizes.^{70–73} Therefore, SEC31A glycosylation may modulate protein–protein interactions and/or transport carrier size in the mammalian COPII outer coat. Taken together, these results indicate that site-specific glycosylation is prevalent on COPII proteins and may impact their biochemical functions.

Next, we asked whether dynamic O-GlcNAcylation regulates the COPII pathway. We used immunoprecipitation (IP) and Western blotting (WB), in combination with specific small molecule inhibitors of OGT (SSGlnAc) and OGA (Thiamet-G),^{59,61} to demonstrate that O-GlcNAc cycles on COPII components, including SEC24C and the Trk-fused gene (TFG), a protein required for COPII function *in vivo* in metazoans (Figure 2A).^{13,75–77} These results suggest that dynamic glycosylation may regulate protein secretion. To test this hypothesis, we performed three functional assays to assess the requirement for O-GlcNAc cycling in COPII-dependent trafficking. First, we used a secreted soluble horseradish peroxidase (ssHRP) reporter that traffics through the secretory pathway in a COPII-dependent manner.⁷⁸ ssHRP can be detected in culture supernatants via standard chemiluminescence, providing a quantitative measure of protein secretion.⁷⁸ We found that inhibition of OGT significantly diminished the level of COPII-dependent secretion of ssHRP without reducing the level of intracellular ssHRP expression or cell viability (Figure 2B and Figure S2). Second, we expressed an enhanced green fluorescent protein (eGFP)-tagged temperature-sensitive mutant of the vesicular stomatitis virus glycoprotein (tsVSVG-eGFP) in mammalian cells.^{79,80} At the nonpermissive temperature, tsVSVG-eGFP is retained in the ER, as indicated by reticular green fluorescence and colocalization with genetically encoded organelle markers (Figure 2C and Figure S3A).^{79,80} Upon shifting to the permissive temperature, tsVSVG-eGFP transits to the Golgi in a strictly COPII-dependent manner, displaying characteristic juxtanuclear punctate fluorescence, thereby providing a live cell assay for pathway function (Figure 2C and Figure S3A).^{79,80} We found that inhibition of OGA markedly delayed COPII-dependent tsVSVG-eGFP trafficking (Figure 2C and Figure S3B). Third, we asked whether O-GlcNAcylation affects the subcellular distribution of COPII proteins. All components of the inner and outer COPII coats exist in both soluble cytoplasmic and membrane-associated pools, and reversible membrane association is required for normal COPII function.^{4–6} To determine whether O-GlcNAc regulates the membrane association of COPII components, we used digitonin treatment to permeabilize the plasma membranes of human cells, permitting the separation of soluble cytoplasmic proteins and membrane-associated proteins,⁸¹ and then performed WB for COPII components on these subcellular fractions. Interestingly, we found that inhibition of OGA reduced the ratio of membrane-associated cytoplasmic SEC23A and SEC31A, indicating that O-GlcNAc cycling regulates the subcellular distribution of essential COPII components (Figure 2D and Figure S4). Together, these results indicate that dynamic O-GlcNAcylation is required for normal COPII-dependent secretion.

Like other PTMs, O-GlcNAc can exert diverse biochemical effects on its substrates, including altering protein conformation or subcellular localization, or mediating or disrupting protein–protein interactions.^{53,54,57,58,82,83} Elegant biochemical and structural studies have revealed that numerous precise protein–protein interactions are required for COPII coat formation, cargo loading, membrane curvature, and scission.^{4–6}

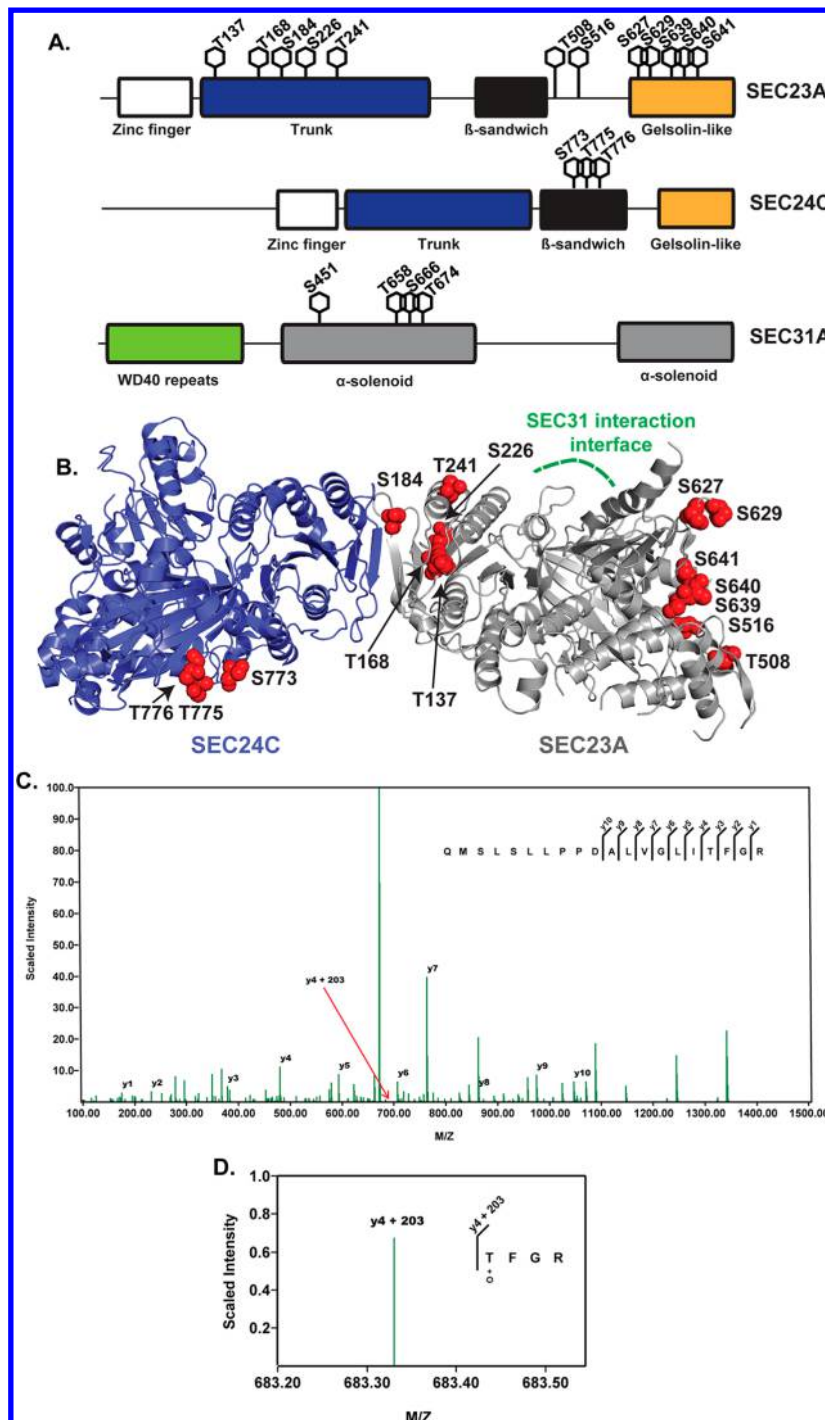


Figure 1. (A) Schematic depicting 12, three, and four O-GlcNAc sites identified on SEC23A, SEC24C, and SEC31A, respectively. Selected domains of each protein are also illustrated. Each modification shown here was unambiguously assigned to a single residue via manual inspection of MS data. Additional information and spectral data for all candidate O-GlcNAc sites are given in Figure S1. (B) The unambiguously assigned O-GlcNAc sites identified in this report are colored red on a model of human SEC23A (silver, Protein Data Bank entry 5VNO) and SEC24C (blue, Protein Data Bank entry 3EH2). The SEC31 interaction interface of SEC23A⁷⁴ is colored green. (C) Representative MS/MS fragmentation spectrum of a SEC23 glycopeptide. Accurate mass measurements of the intact $_{[152]}^{\text{QMSLSLLPPDALVGLITFGR}}_{[171]}$ peptide indicated the presence of two O-GlcNAc modifications. HCD fragmentation revealed a y-ion series through y10 (ALVGLITFGR fragment) as well as a fragmentation series y4 (TFGR fragment) plus 203.0794 Da, which is highlighted by y4 + 203 and expanded in panel D. (D) Fragmentation series with an intact O-GlcNAc modification (magnified from the spectrum in panel C). This fragment ion series localizes one O-GlcNAc modification (denoted +O) unambiguously to Thr168, with either Ser154 or Ser156 as the additional site. All O-GlcNAc sites depicted in panels A and B were unambiguously assigned using similar analysis, or because the number of O-GlcNAc moieties detected equaled the number of Ser/Thr residues on a given tryptic peptide.

In addition, our MS site mapping data demonstrate that O-GlcNAcylation occurs on known or predicted protein–protein interaction domains of COPII components (Figure 1 and Figure S1).

Therefore, we hypothesized that O-GlcNAc may mediate the protein–protein interactions of COPII components. However, physiologically important O-GlcNAc-mediated protein–protein

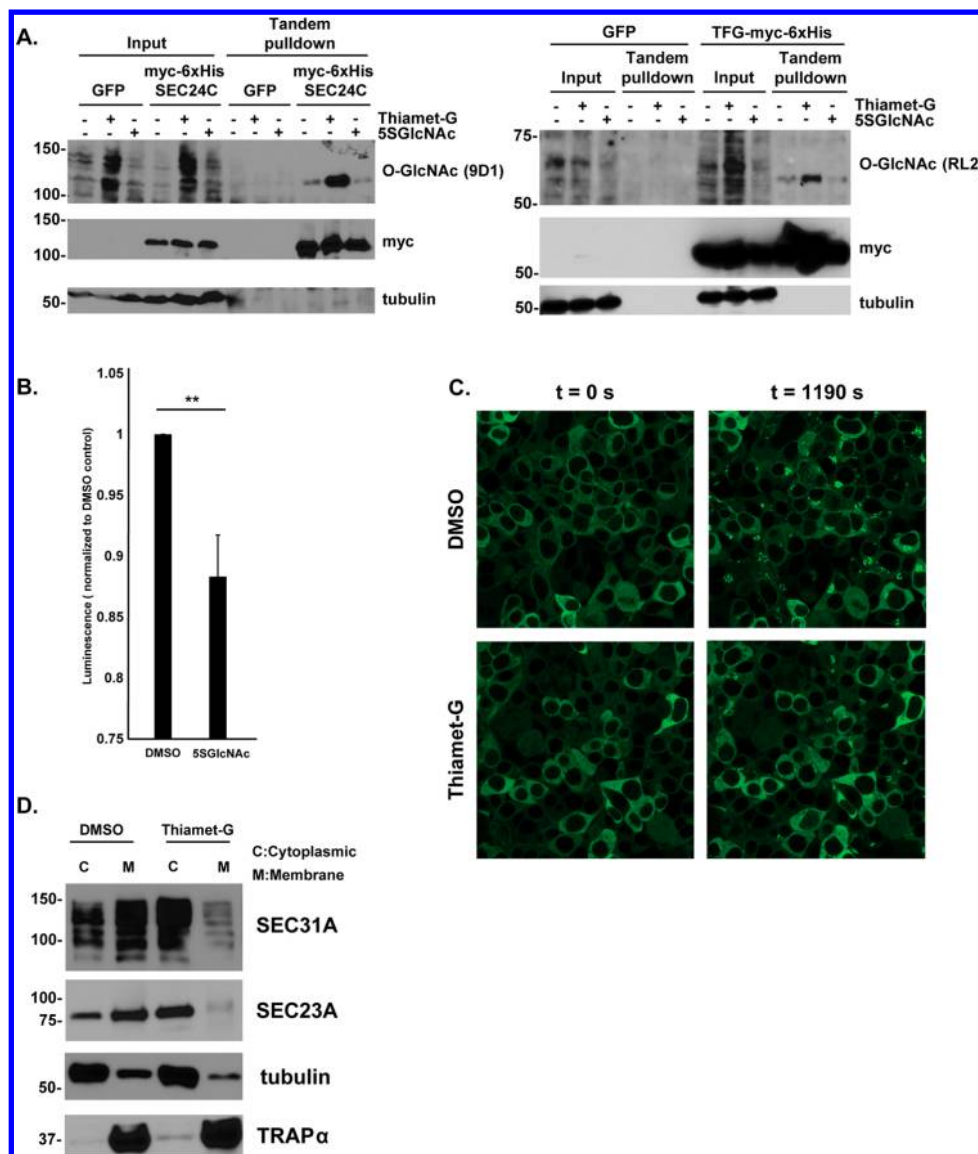


Figure 2. (A) O-GlcNAc dynamically modifies COPII components. 293T-17 cells were transfected with either myc-6xHis-SEC24C or TFG-myc-6xHis and treated with vehicle (DMSO), 25 μ M Thiamet-G, or 25 μ M 5SGlcNAc 8 h prior to being harvested. Tandem affinity-purified SEC24C and TFG were analyzed by WB. Both proteins demonstrated O-GlcNAc cycling as indicated by an increase in the intensity of the signal upon being treated with Thiamet-G, and a decrease in the intensity of the signal with 5SGlcNAc, compared to that of the vehicle. (B) 293T cells were treated with vehicle (DMSO) or 50 μ M 5SGlcNAc and transfected with ssHRP. The amount of ssHRP in the medium supernatant was measured after 20 h via a luminescence assay. Inhibition of OGT via 5SGlcNAc significantly diminished the rate of secretion. $n = 6$; $** p = 0.006$, Student's t test. Error bars are standard errors of the mean. (C) COS7 cells stably expressing tsVSVG-eGFP were treated with vehicle (DMSO) or 25 μ M Thiamet-G for 8 h at the nonpermissive temperature (40 $^{\circ}$ C) and then shifted to the permissive temperature (32 $^{\circ}$ C). Cells were imaged every 10 s for 20 min, monitoring the movement of tsVSVG-eGFP from ER (reticular ER fluorescence) to the Golgi (juxtannuclear punctate fluorescence). See also Figure S3. (D) SW1353 cells were incubated with DMSO or 50 μ M Thiamet-G for 24 h. Cytoplasm (C) and endomembrane (M) fractions were prepared by digitonin fractionation, and SEC23A and SEC31A were analyzed by WB. Tubulin and TRAP α serve as loading controls for cytoplasmic and integral ER transmembrane proteins, respectively. One representative experiment is shown. Similar results were obtained in three independent biological replicates (Figure S4).

interactions can be substoichiometric, transient, and low-affinity, presenting a significant challenge for their characterization.^{53,54,57,58,82,83} To address this challenge, we harnessed a chemical biology method to covalently capture O-GlcNAc-mediated protein–protein interactions in live human cells.⁶⁰ In this strategy, cells are metabolically labeled with a GlcNAc analogue bearing a diazirine photo-cross-linking moiety, termed “GlcNDaz”.⁶⁰ GlcNDaz is accepted by the GlcNAc salvage pathway, converted to UDP-GlcNDaz, and used by OGT to

decorate its native substrates.⁶⁰ A brief UV treatment of GlcNDaz-labeled cells triggers the covalent cross-linking of O-GlcNDaz moieties to any binding partner proteins within $\sim 2\text{--}4$ Å of the sugar.⁶⁰ Because of this short radius, GlcNDaz cross-linking occurs exclusively at sites where the glycan contributes to the interaction interface, without cross-linking to distant or nonspecific proteins.⁶⁰ These covalent cross-links can be conveniently visualized through the GlcNDaz-dependent appearance of high-molecular weight species on a Western blot

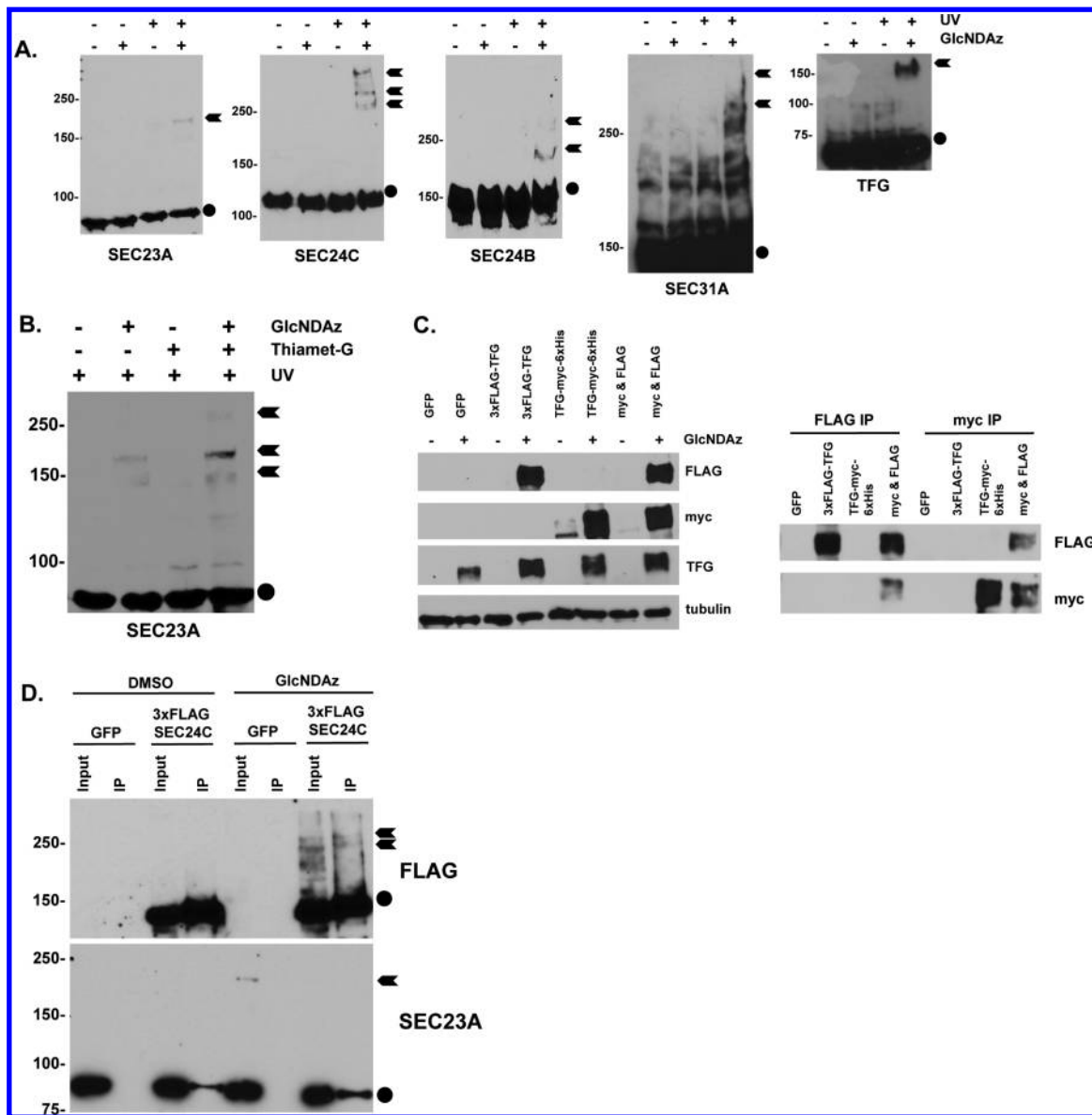


Figure 3. (A) HeLa/UAP1 or 293T/UAP1 cells were treated with 100 μ M GlcNDAz or vehicle (DMSO) and UV light (or not), and lysates were analyzed by WB. Circles indicate un-cross-linked proteins running at their predicted molecular weights. Arrows indicate GlcNDAz- and UV-dependent cross-linked species. (B) HeLa/UAP1 cells were treated with 100 μ M GlcNDAz, 50 μ M Thiamet-G, vehicle (DMSO), and UV light as indicated for 24 h, and lysates were analyzed by WB. Circle indicates un-cross-linked SEC23A running at its predicted molecular weight. Arrows indicate GlcNDAz- and UV-dependent cross-linked species. (C) In the left panel, 293T/UAP1 cells were transfected with GFP (control), 3xFLAG-TFG only, or TFG-myc-6xHis only or co-transfected with both FLAG and myc-6xHis constructs (“myc & FLAG”). Then, cells were treated with DMSO (vehicle) only or 100 μ M GlcNDAz and exposed to UV light. Lysates were analyzed by WB, confirming that both myc- and FLAG-tagged TFG cross-links like endogenous TFG in a GlcNDAz-dependent manner. Covalently cross-linked bands of TFG (~150 kDa) are shown. In the right panel, 293T/UAP1 cells were transfected with GFP (control), 3xFLAG-TFG only, or TFG-myc-6xHis only or co-transfected with both FLAG and myc-6xHis constructs (“myc & FLAG”). Then, cells were treated with 100 μ M GlcNDAz and UV light, and lysates were analyzed by IP and WB as indicated. Covalently cross-linked bands of TFG (~150 kDa) are shown. (D) 293T/UAP1 cells were transfected with 3xFLAG-SEC24C or GFP (control) and treated with 100 μ M GlcNDAz or vehicle. Lysates were analyzed by anti-FLAG IP and WB. Cross-linked complexes of 3xFLAG-SEC24C were successfully purified (lane 8) but did not contain SEC23A. Notably, endogenous un-cross-linked SEC23A co-immunoprecipitates with SEC24C (lanes 4 and 8), but endogenous cross-linked SEC23A (lane 5) does not, demonstrating that SEC24C and SEC23A each cross-link, but not to each other. Circles indicate un-cross-linked proteins running at their predicted molecular weights. Arrows indicate GlcNDAz- and UV-dependent cross-linked species.

for the protein of interest. Therefore, GlcNDAz is a powerful chemical tool for identifying direct, glycosylation-mediated interactions between endogenous proteins in live cells.⁶⁰

Using GlcNDAz, we found that endogenous SEC23A, SEC24B, SEC24C, SEC31A, and TFG all engage in O-GlcNAc-mediated protein–protein interactions in multiple human cell lines, detected as massive cross-links on a Western blot (Figure 3A).

Importantly, GlcNDAz cross-linking of SEC23A was enhanced when deglycosylation was blocked by brief Thiamet-G treatment (Figure 3B), indicating that these interactions are dynamic and O-GlcNAc-specific. We concluded that O-GlcNAc mediates regulated interactions of COPII proteins.

To test the hypothesis that O-GlcNAc might mediate some of the well-characterized protein–protein interactions in the

COPII coat,^{4–6} we examined TFG, SEC23A, and SEC24C as model COPII glycoproteins. TFG homo-oligomerizes *in vitro* and in cells, and this property is required for its subcellular localization and function in COPII cargo trafficking.^{13,75–77}

To determine whether O-GlcNAc participates in homotypic TFG–TFG interactions inside cells, we created constructs of human TFG with different epitope tags. IP/WBs with these constructs revealed that covalent, GlcNDAz-dependent cross-linked complexes of TFG contain both tagged versions of TFG simultaneously (Figure 3C). These results demonstrate that the GlcNDAz-dependent complexes are homo-oligomers, suggesting that O-GlcNAc may participate in TFG–TFG interactions in live cells.

Next, we examined the potential involvement of O-GlcNAc in the heterodimerization of SEC23 and SEC24, an essential step in the formation of the COPII prebudding complex.^{4–6} We expressed FLAG-SEC24C in human cells and observed GlcNDAz-dependent cross-linking similar to that of endogenous SEC24C (Figure 3A,D). We immunoprecipitated SEC24C and performed WB for candidate interactors, including SEC23A (Figure 3D), SEC13, SEC31, SARI, and the scaffolding protein SEC16 (not shown). In all cases, we failed to detect any candidate interactors in the cross-linked SEC24C complexes (Figure 3D and not shown). Notably, endogenous SEC23A again cross-linked in this context, though not to SEC24C (Figure 3D). Similarly, immunoprecipitated GlcNDAz cross-links of SEC23A did not contain SEC24, SEC13, SEC31, or SARI (not shown). We concluded that SEC23A and SEC24C engage in specific but distinct O-GlcNAc-mediated protein–protein interactions, which may influence COPII trafficking. Altogether, these results demonstrate that dynamic O-GlcNAcylation mediates both known and novel interactions among COPII pathway proteins.

We next focused on SEC23A, because SEC23 is an essential COPII component,^{4–6,10,84} and because human SEC23A mutations cause CLSD.^{15,21,26} To further elucidate the biochemical effects of SEC23A O-GlcNAcylation, we created unglycosylatable point mutants (Ser/Thr → Ala) in 16 of the candidate sites we detected by MS, focusing on residues that are highly conserved across evolution (Figure 1A and Figure S1): S97, S102, S115, S116, T137, T168, S184, S226, T241, S508, S516, S627, S629, S639, S640, and S641. We expressed wild type or point mutant SEC23A constructs in human cells and performed GlcNDAz cross-linking (Figure 4A). We found that the S115A, S116A, T137A, T168A, and S184A mutants weakened or abrogated GlcNDAz-mediated cross-linking, whereas the others did not (Figure 4A). Interestingly, three of the residues required for SEC23A cross-linking, T137, T168, and S184, lie near its SEC24 binding interface (Figure 1A,B). However, as noted, SEC24 is not the GlcNDAz-mediated cross-linked partner of SEC23 (Figure 3). These observations suggest that the site-specific O-GlcNAcylation of SEC23A near the SEC24 binding interface mediates an interaction distinct from that of the SEC23/SEC24 prebudding complex.

We next investigated the functional significance of site-specific SEC23A glycosylation in a human cell system. Chondrocytes create and maintain cartilage, largely through the regulated secretion of collagen,⁸⁵ and SEC23A is required for this process *in vivo*.^{15,21,26} To assess the function of SEC23A with a physiologically relevant cell system and model cargo, we used CRISPR/Cas9 methods to delete the endogenous SEC23A gene in SW1353 human chondrosarcoma cells (Figure S5), which secrete endogenous collagen.^{86,87} Complete loss of

SEC23A caused intense collagen accumulation and distended ER morphology (Figures S6 and S7), which resemble the reported previously COPII cargo defects of CLSD patient cells.^{15,21,26} These observations confirm that SEC23A^{−/−} SW1353 cells are an appropriate system for testing the function of unglycosylatable SEC23A mutants in trafficking endogenous collagen. Next, we stably re-expressed empty vector, wild type SEC23A, or unglycosylatable single-point mutant SEC23A alleles. To create an appropriately sensitive assay for SEC23A function, we knocked down SEC23B (Figure S8), preventing compensation from this paralog, as described previously.⁶⁶ We then assessed SEC23A function in these reconstituted cell lines by tracking collagen secretion via immunofluorescence (IF) microscopy. Interestingly, SEC23A^{−/−} SW1353 cells reconstituted with the S184A unglycosylatable point mutant exhibited a significantly higher proportion of retained collagen and a characteristic dilated ER morphology, as compared to cells reconstituted with wild type SEC23A, despite partial rescue (Figure 4B,C). Importantly, however, wild type and S184A mutant SEC23A co-immunoprecipitated endogenous SEC24 proteins with similar efficiencies (Figure S9A), indicating that the trafficking defect we observe in the S184A mutant (Figure 4B,C) is not due to gross protein misfolding or lost SEC24 binding. Together, these results demonstrate that the S184 glycosylation site of SEC23A is required for its collagen trafficking function in human chondrosarcoma cells, possibly because of post-translational regulation at the SEC23A/SEC24 interface.

In developing vertebrates, collagen trafficking and skeletogenesis are stringently dependent on SEC23A, because SEC23A partial loss-of-function mutations cause CLSD in humans and similar phenotypes in model organisms.^{15,18,21,26,27,88–90} Our biochemical and cellular data (Figures 1–4) suggest that site-specific O-GlcNAcylation might regulate SEC23A function in developing tissues. To test this hypothesis, we took advantage of a vertebrate model of SEC23A dysfunction.^{18,27} We have shown previously that mutations in zebrafish *sec23a* underlie the *crusher* phenotype, exhibiting collagen mis-trafficking, chondrocyte failure, and skeletal dysmorphology^{18,27} that closely resemble CLSD1.^{5,21,26} Therefore, *crusher* fish provide a valuable vertebrate genetic model for studying SEC23A function *in vivo*.^{18,27} Importantly, the human and zebrafish SEC23A proteins are 91% identical, and all but one (S629) of the 16 putative O-GlcNAc sites that we examined (Figure 4A) are conserved among these orthologs.

We tested the functional importance of SEC23A O-GlcNAcylation sites *in vivo* using the *crusher* model. First, we confirmed that wild type zebrafish SEC23A cross-links in our GlcNDAz assay like its human ortholog (Figure 5A). Then, we designed a compound mutant SEC23A allele, in which four residues required for GlcNDAz cross-linking and conserved from humans to fish (S115, S116, T137, and T168) were mutated to alanine (“4A mutant”). We created expression constructs of the human and zebrafish SEC23A 4A mutant and confirmed that they are defective in GlcNDAz-mediated cross-linking (Figure 5A). These results indicate that the O-GlcNAc-mediated interactions of SEC23A are biochemically conserved across vertebrates.

Next, we developed an *in vivo* assay of SEC23A function in skeletogenesis (Figure 5B). We expressed wild type or 4A mutant SEC23A in *sec23a*-deficient (*crusher*) zebrafish chondrocytes and tracked COPII-dependent collagen transport by immunohistochemistry (Figure 5B). We measured the cytosolic area occupied by collagen as an established marker

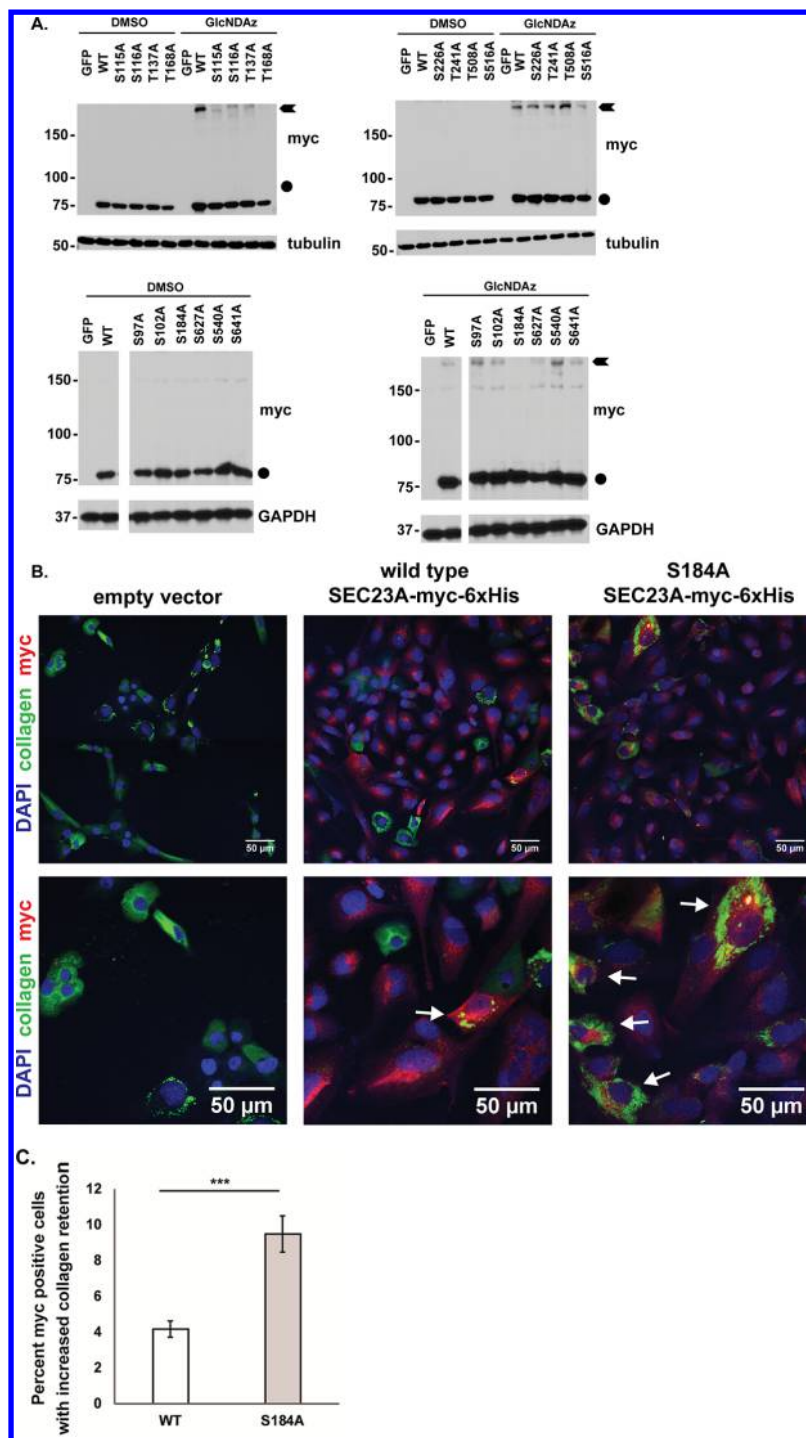


Figure 4. (A) 293T/UAP1 cells were transfected with plasmids encoding GFP (control), wild type SEC23A-myc-6xHis, or the indicated SEC23A-myc-6xHis point mutants. Cells were treated with vehicle (DMSO) or 100 μ M GlcNDAz and irradiated with UV light. Lysates were analyzed by WB. The S115A, S116A, T137A, T168A, and S184A mutants all show a marked reduction in their level of cross-linking. Circles indicate un-cross-linked SEC23A running at its predicted molecular weight. Arrows indicate GlcNDAz- and UV-dependent cross-linked species. White rectangles indicate where irrelevant lanes have been cropped out of a single blot (bottom panels). Duplicate wild type SEC23A cross-linked samples were run on multiple blots due to space constraints. Therefore, apparent variability in the wild type cross-linking efficiency is due to blot-to-blot variation in enhanced chemiluminescence detection. (B) SEC23A^{-/-} SW1353 cells stably reconstituted with the empty vector (left), wild type SEC23A-myc-6xHis (middle), or S184A SEC23A-myc-6xHis (right) were transfected with anti-SEC23B siRNA [or scrambled SEC23B siRNA (not shown)] and treated with 50 μ g/mL sodium ascorbate for 7 h to induce collagen translation.^{46,47} Then, cells were fixed and stained for SEC23A (anti-myc, red), endogenous collagen (LF68 anti-collagen, green), and DNA (DAPI, blue). Cells exhibiting both SEC23A expression and aberrant ER collagen staining (white arrows) were quantified as a fraction of the total number of SEC23A-positive cells. Representative images from eight biological replicates are shown at two magnifications (top and bottom panels). (C) Quantification of IF data presented in panel B. Cells expressing S184A SEC23A were more than twice as likely to exhibit retained collagen, compared to those expressing wild type SEC23A. $n = 8$; *** $p < 0.001$, Student's t test. Error bars are standard errors of the mean.

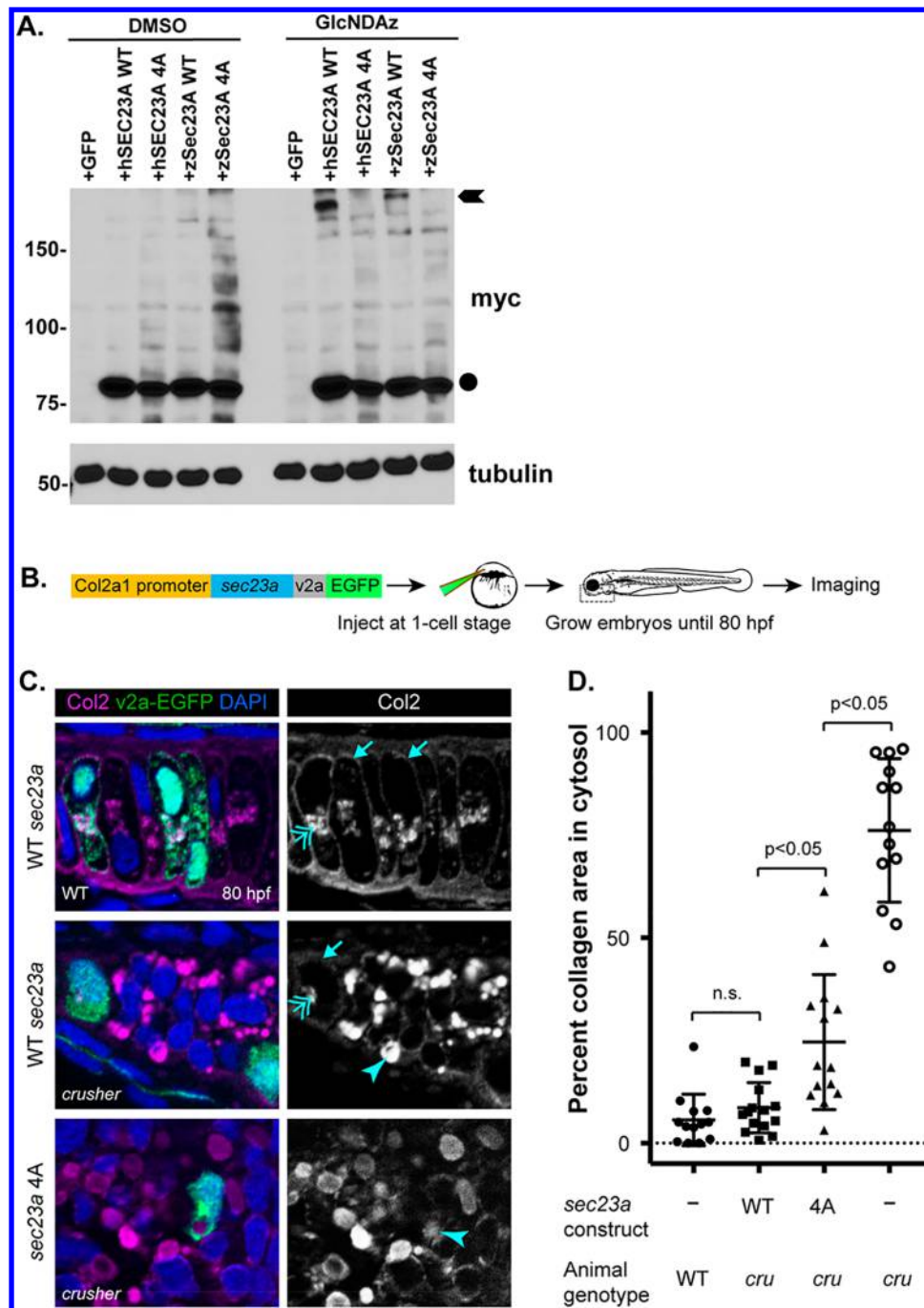


Figure 5. (A) 293T/UAP1 cells were transfected with either GFP (control), human wild type SEC23A-myc-6xHis, zebrafish wild type Sec23A-myc-6xHis, or zebrafish 4A Sec23A-myc-6xHis. Circle indicates un-cross-linked SEC23A running at its predicted molecular weight. Arrows indicate GlcNDaz- and UV-dependent cross-linked species. The 4A mutations reduce the level of cross-linking in both human and zebrafish SEC23A. (B) Experimental strategy for mosaic expression of Sec23A in zebrafish chondrocytes. Wild type Sec23A or the 4A mutant was expressed under the zebrafish Col2a1 promoter. Embryos injected with Sec23A constructs were grown until 80 h postfertilization (hpf) and cryosectioned for immunohistochemistry. (C) Cells expressing Sec23A constructs are marked by v2a-EGFP. Wild type cells secrete collagen to the extracellular space (arrows, top panel), whereas intracellular collagen accumulates in *crusher* (*sec23a* loss-of-function) mutant chondrocytes (arrowhead, middle panel). Overexpression of wild type Sec23A in *crusher* animals leads to clearance of intracellular collagen, whereas expression of the Sec23A 4A mutant fails to do so (arrowhead, bottom panel). Double-headed arrows point to normal levels of collagen in the secretory compartment. (D) Quantification of zebrafish rescue experiments. The percent of cell area occupied by collagen shows that wild type Sec23A expression in *crusher* chondrocytes restores collagen secretion to normal levels, whereas the Sec23A 4A mutant does not, despite partial rescue. The highest level of intracellular collagen occurs in *crusher* (*cru*) chondrocytes. The investigator was blinded to the wild type or 4A mutant genotype while performing quantification, per standard practice.^{18,27,28} $p < 0.05$, Student's *t* test. Error bars are standard errors of the mean.

of its intracellular retention.^{18,27,28} We found that 5% of the cytosolic area of wild type chondrocytes was occupied by collagen 80 h postfertilization (hpf), which corresponds to

normal collagen traffic within secretory pathway compartments (Figure 5C,D). In contrast, 50–95% of the cytosolic area of *sec23a*-deficient chondrocytes was filled with aberrantly

retained collagen (Figure 5C,D), consistent with our prior reports.^{18,27} Interestingly, while the expression of wild type SEC23A in *crusher* chondrocytes restored collagen secretion to wild type levels in a cell-autonomous fashion, the unglycosylatable SEC23A 4A mutant only partially restored collagen secretion, exhibiting levels of collagen retention significantly higher than that of the wild type (Figure 5C,D). Together, these results suggest that site-specific O-GlcNAcylation of SEC23A may regulate the *in vivo* COPII-dependent transport of SEC23A-dependent cargoes, including collagen.

DISCUSSION

The COPII trafficking pathway is essential for cell and tissue physiology in vertebrates and is dysregulated in several human diseases. While the core COPII machinery is relatively well understood, little is known about how trafficking is dynamically regulated in response to physiological or pathological cues. Our results indicate that O-GlcNAcylation of COPII proteins may be one important mode of pathway regulation in vertebrates.

We have shown that O-GlcNAc is a prevalent modification of COPII proteins, including SEC23, SEC24, SEC31, and TFG (Figures 1, 2A, and 3A). Like phosphorylation, O-GlcNAcylation can exert a wide range of biochemical effects on its substrates, and it will be important to delineate the effects of COPII protein glycosylation at each individual modification site to build an integrated model for how O-GlcNAc affects protein trafficking from the ER. As a first step toward this goal, our GlnDaz results suggest that O-GlcNAc moieties lie at or very close to the interaction interface between TFG monomers, indicating a potential biochemical function for TFG glycosylation (Figure 3A,C). The N-terminal half of TFG, comprising its PB1 and coiled-coil domains, mediates homooligomerization, and this property is required for its trafficking function *in vivo*.^{13,75–77} While unglycosylated TFG can homooligomerize *in vitro*, our results suggest that O-GlcNAcylation may facilitate or regulate this process in live cells.^{13,77} Similarly, we show that both SEC23A and SEC24C also engage in O-GlcNAc-mediated protein–protein interactions, but not with each other, or with several other known binding partners in the COPII system (Figure 3A,B,D). These data suggest that novel O-GlcNAc-mediated protein–protein interactions may govern SEC23 and/or SEC24 function in the COPII system. It will be important to determine in future work how changes in site-specific glycosylation of TFG, SEC23, or SEC24 directly affect their biochemical activities *in vivo*.

At the cellular level, our results indicate that O-GlcNAc cycling in general (Figure 2) and specific SEC23A glycosylation sites in particular (Figure 4B,C) are required for COPII-dependent protein secretion. Because native PTMs, including O-GlcNAc, are not essential for *in vitro* COPII vesicle assembly from minimal components,⁹¹ it is likely that O-GlcNAcylation and other PTMs are instead required to modulate the activity of the pathway *in vivo*. The precise molecular events affected by O-GlcNAc and the full complement of substrates and modification sites most critical for this regulation remain incompletely understood. Interestingly, however, OGA inhibition both delayed the trafficking of tsVSVG-eGFP (Figure 2C) and decreased the size of the pools of membrane-associated SEC23A and SEC31A (Figure 2D). These results suggest that unfettered O-GlcNAc cycling may be required for the efficient recruitment or recycling of COPII proteins to the ER or Golgi membranes. Other PTMs govern COPII in this way.

For example, Golgi-localized kinase CK1 δ and phosphatase PP6 act reciprocally on SEC23 and SEC24 to ensure orderly COPII carrier budding, fusion, and directionality,^{38,39} and a recent study demonstrated that phosphorylation by CK2 inhibits the membrane association of SEC31.⁴⁴

Notably, O-GlcNAc and O-phosphate exhibit a complex interplay in cells, frequently competing for nearby or identical residues on a given protein and exerting antagonistic effects.⁵⁴ Indeed, a prior report suggests that the cell cycle-dependent phosphorylation and glycosylation of SEC24 are reciprocal and may affect its membrane association.⁵⁰ Our data are consistent with this proposed model, but additional cell biological studies with unglycosylatable point mutants of COPII proteins will be required to elucidate the responsible modification sites and potential O-GlcNAc/O-phosphate cross-talk. In the case of SEC23A, none of the glycosylation sites that we examined (Figure 4A) is reported to be phosphorylated, though additional sites of both modifications may yet await discovery. In contrast, phosphorylation of S773 and T776 of SEC24C has been reported,⁹² suggesting that the interplay between O-GlcNAcylation and phosphorylation at these sites could tune COPII activity. Future studies will address the potential cross-talk among PTMs of COPII proteins.

The COPII system of vertebrates is significantly more complex than that of lower eukaryotes. For example, vertebrates possess two paralogs of SEC23 (A and B) and four paralogs of SEC24 (A–D), whereas budding yeast has one essential ortholog of each. The functional significance of vertebrates' multiple COPII paralogs remains largely unclear. All four SEC24 paralogs exhibit analogous biochemical functions in early COPII coat formation and cargo capture, yet mouse knockout studies and differences in cargo binding clearly indicate distinct, if overlapping, physiological functions among these proteins.^{17,28,93–95} Studies of SEC23A and SEC23B revealed analogous results, despite their high level of conservation and similar biochemical functions.^{96–99} Currently, it is not well understood how these COPII components achieve distinct biological roles *in vivo*, though tissue-specific expression patterns of paralogs and cargoes likely contribute.^{89,90} Another possibility is that PTMs differentially regulate COPII paralogs. Consistent with this notion, we observed distinct GlnDaz cross-links of endogenous SEC24B and SEC24C (Figure 3A), suggesting that O-GlcNAcylation may mediate different protein–protein interactions among paralogs. In addition, one glycosylation site that we mapped on human SEC24C (T775) is conserved as a serine or threonine in all four human SEC24 paralogs, whereas the other two localized SEC24C O-GlcNAc sites (Figure 1A,B) and several candidate sites (Figure S1) are conserved in only one or none of the other three SEC24 paralogs. Therefore, glycosylation of multiple SEC24 paralogs at the T775 cognate site may impact all COPII traffic, whereas glycosylation of SEC24C at other sites may provide paralog-specific regulation to tune the trafficking of specific cargoes or cell types. In contrast, of the 12 unambiguously localized O-GlcNAc sites we identified on human SEC23A (Figure 1A,B), all except S516 are conserved in SEC23B (with a serine in SEC23B corresponding to SEC23A T508). These results suggest that glycosylation could affect SEC23 paralogs more uniformly than SEC24 paralogs, though this hypothesis remains to be tested.

Finally, our results demonstrate that several evolutionarily conserved glycosylation sites on SEC23A are required for O-GlcNAc-mediated protein–protein interactions in cells, and

to support collagen secretion in SW1353 cells and skeletogenesis in developing zebrafish (Figures 4 and 5). One of these residues, S184, lies near the SEC23/SEC24 interface, potentially providing a site for a regulatory O-GlcNAc-mediated protein–protein interaction with a protein other than SEC24 (Figures 3D and 4A). In contrast, the residues altered in the SEC23A 4A mutant do not lie exclusively at the SEC23/SEC24 interface, and O-GlcNAcylation may play a biochemically distinct role at those sites. Although our cell- and animal-based experiments (Figures 2, 4, and 5) cannot stringently rule out the possibility that the S184A or 4A mutation induces a deleterious conformational change in SEC23A, both mutants co-immunoprecipitate with SEC24 proteins with efficiencies similar to that of wild type SEC23A, arguing against a dramatic conformational change or misfolding (Figure S9A,B). Similarly, neither SEC23A deletion nor OGT or OGA inhibition disrupted ER exit sites (ERES), as judged by IF staining of the endogenous, canonical ERES marker SEC16 (Figure S10). This result suggests that the functional effects that we observe upon OGT or OGA inhibition (Figure 2) or ablation of SEC23A glycosylation sites (Figure 4) may be due to regulation of SEC23A and/or other COPII proteins downstream of ERES formation. Therefore, we propose that SEC23A O-GlcNAcylation at these sites is required to regulate its interaction with binding partners beyond SEC24. We expect that future GlcNAz cross-linking and MS proteomic experiments that aim to identify the O-GlcNAc-dependent binding partner(s) of SEC23A will facilitate the elucidation of the molecular mechanisms through which site-specific O-GlcNAcylation of SEC23A influences COPII trafficking.

At the organismal level, our results suggest that dynamic O-GlcNAcylation of SEC23A may govern collagen trafficking during vertebrate development (Figures 4 and 5). Consistent with this idea, recent work identified a connection between whole-body O-GlcNAc levels and chondrogenic differentiation in mice,¹⁰⁰ implicating O-GlcNAcylation in skeletogenesis. We have also shown that O-GlcNAc modifies SEC24C and SEC31A (Figure 1), both of which may participate in efficient *in vivo* collagen secretion, as well.^{46,47,101} Therefore, O-GlcNAcylation may be a conserved mode of COPII regulation in chondrocytes during vertebrate development. Testing this hypothesis will be an important goal of future studies.

■ ASSOCIATED CONTENT

● Supporting Information

The Supporting Information is available free of charge on the ACS Publications website at DOI: 10.1021/acs.biochem.7b00870.

Summary of MS data and identified O-GlcNAc sites (Figure S1), effect of 5SGlcNAc on the ssHRP assay (Figure S2), organelle marker and Thiamet-G controls for the tsVSVG-eGFP assay (Figure S3), digitonin fractionation replicates and densitometry quantification (Figure S4), validation of SEC23A deletion by CRISPR/Cas9 (Figure S5), accumulation of collagen in SEC23A^{-/-} cells (Figure S6), distended ER morphology in SEC23A^{-/-} cells (Figure S7), validation of SEC23B^{-/-} depletion by siRNA (Figure S8), SEC23A S184A and 4A co-IPs with SEC24 paralogs (Figure S9), and lack of an effect on ERES by SEC23A deletion or OGT/OGA inhibition (Figure S10) (PDF)
Scaffold file containing SEC23A, SEC24C, and SEC31A spectra used for site mapping (ZIP)

■ AUTHOR INFORMATION

Corresponding Author

*E-mail: michael.boyce@duke.edu.

ORCID

Nathan J. Cox: 0000-0002-8573-5596

Michael Boyce: 0000-0002-2729-4876

Author Contributions

N.J.C., B.J.B., T.R.M., B.C., P.M.L., T.J.S., and A.C. performed all experiments conducted in mammalian cells. G.U. performed the zebrafish experiments. E.J.S. performed MS-based O-GlcNAc site mapping of COPII proteins. M.H. and A.A. designed and tested conditions for SEC23B knockdown. N.J.C., G.U., B.J.B., T.R.M., B.C., A.A., E.W.K., and M.B. designed the experiments, analyzed the data, and interpreted the results. E.W.K. supervised the zebrafish experiments. M.B. supervised all aspects of the work. N.J.C. and M.B. wrote and revised the manuscript. All authors reviewed and approved the finished manuscript.

Funding

This work was supported by a Scholar Award from the Rita Allen Foundation, a Research Grant from the Mizutani Foundation, National Institutes of Health Grants R01GM117473 (to M.B.), R01HL092217-06 (to E.W.K.), and R01GM110567 (to A.A.), the Vanderbilt International Scholar Program, and American Heart Association Predoctoral Fellowship 15PRE22940041 (to G.U.).

Notes

The authors declare no competing financial interest.

■ ACKNOWLEDGMENTS

The authors thank Frederic Bard, Larry Fisher, Josh Gamse, David Ginsburg, Rami Khoriaty, Jennifer Kohler, Chris Nicchitta, Randy Schekman, and Benjamin Swarts for antibodies or plasmids and David Gooden of the Duke Small Molecule Synthesis Facility for chemical synthesis.

■ REFERENCES

- (1) Huh, W. K., Falvo, J. V., Gerke, L. C., Carroll, A. S., Howson, R. W., Weissman, J. S., and O'Shea, E. K. (2003) Global analysis of protein localization in budding yeast. *Nature* 425, 686–691.
- (2) Kaufman, R. J. (1999) Stress signaling from the lumen of the endoplasmic reticulum: coordination of gene transcriptional and translational controls. *Genes Dev.* 13, 1211–1233.
- (3) Barlowe, C. K., and Miller, E. A. (2013) Secretory protein biogenesis and traffic in the early secretory pathway. *Genetics* 193, 383–410.
- (4) Miller, E. A., and Schekman, R. (2013) COPII - a flexible vesicle formation system. *Curr. Opin. Cell Biol.* 25, 420–427.
- (5) Routledge, K. E., Gupta, V., and Balch, W. E. (2010) Emergent properties of proteostasis-COPII coupled systems in human health and disease. *Mol. Membr. Biol.* 27, 385–397.
- (6) Brandizzi, F., and Barlowe, C. (2013) Organization of the ER-Golgi interface for membrane traffic control. *Nat. Rev. Mol. Cell Biol.* 14, 382–392.
- (7) Baker, D., Hicke, L., Rexach, M., Schleyer, M., and Schekman, R. (1988) Reconstitution of SEC gene product-dependent intercompartmental protein transport. *Cell* 54, 335–344.
- (8) Ruohola, H., Kabcenell, A. K., and Ferro-Novick, S. (1988) Reconstitution of protein transport from the endoplasmic reticulum to the Golgi complex in yeast: the acceptor Golgi compartment is defective in the sec23 mutant. *J. Cell Biol.* 107, 1465–1476.
- (9) Barlowe, C., Orci, L., Yeung, T., Hosobuchi, M., Hamamoto, S., Salama, N., Rexach, M. F., Ravazzola, M., Amherdt, M., and Schekman,

- R. (1994) COPII: a membrane coat formed by Sec proteins that drive vesicle budding from the endoplasmic reticulum. *Cell* 77, 895–907.
- (10) Fromme, J. C., Orci, L., and Schekman, R. (2008) Coordination of COPII vesicle trafficking by Sec23. *Trends Cell Biol.* 18, 330–336.
- (11) Paczkowski, J. E., Richardson, B. C., and Fromme, J. C. (2015) Cargo adaptors: structures illuminate mechanisms regulating vesicle biogenesis. *Trends Cell Biol.* 25, 408–416.
- (12) Khoriaty, R., Vasievich, M. P., and Ginsburg, D. (2012) The COPII pathway and hematologic disease. *Blood* 120, 31–38.
- (13) Beetz, C., Johnson, A., Schuh, A. L., Thakur, S., Varga, R. E., Fothergill, T., Hertel, N., Bomba-Warczak, E., Thiele, H., Nurnberg, G., Altmuller, J., Saxena, R., Chapman, E. R., Dent, E. W., Nurnberg, P., and Audhya, A. (2013) Inhibition of TFG function causes hereditary axon degeneration by impairing endoplasmic reticulum structure. *Proc. Natl. Acad. Sci. U. S. A.* 110, 5091–5096.
- (14) Jones, B., Jones, E. L., Bonney, S. A., Patel, H. N., Mensenkamp, A. R., Eichenbaum-Voline, S., Rudling, M., Myrdal, U., Annesi, G., Naik, S., Meadows, N., Quattrone, A., Islam, S. A., Naoumova, R. P., Angelin, B., Infante, R., Levy, E., Roy, C. C., Freemont, P. S., Scott, J., and Shoulders, C. C. (2003) Mutations in a Sar1 GTPase of COPII vesicles are associated with lipid absorption disorders. *Nat. Genet.* 34, 29–31.
- (15) Boyadjiev, S. A., Fromme, J. C., Ben, J., Chong, S. S., Nauta, C., Hur, D. J., Zhang, G., Hamamoto, S., Schekman, R., Ravazzola, M., Orci, L., and Eyaid, W. (2006) Cranio-lenticulo-sutural dysplasia is caused by a SEC23A mutation leading to abnormal endoplasmic-reticulum-to-Golgi trafficking. *Nat. Genet.* 38, 1192–1197.
- (16) Zhang, B., Cunningham, M. A., Nichols, W. C., Bernat, J. A., Seligsohn, U., Pipe, S. W., McVey, J. H., Schulte-Overberg, U., de Bosch, N. B., Ruiz-Saez, A., White, G. C., Tuddenham, E. G., Kaufman, R. J., and Ginsburg, D. (2003) Bleeding due to disruption of a cargo-specific ER-to-Golgi transport complex. *Nat. Genet.* 34, 220–225.
- (17) Merte, J., Jensen, D., Wright, K., Sarsfield, S., Wang, Y., Schekman, R., and Ginty, D. D. (2010) Sec24b selectively sorts Vangl2 to regulate planar cell polarity during neural tube closure. *Nat. Cell Biol.* 12, 41–46.
- (18) Lang, M. R., Lapierre, L. A., Frotscher, M., Goldenring, J. R., and Knapik, E. W. (2006) Secretory COPII coat component Sec23a is essential for craniofacial chondrocyte maturation. *Nat. Genet.* 38, 1198–1203.
- (19) Schwarz, K., Iolascon, A., Verissimo, F., Trede, N. S., Horsley, W., Chen, W., Paw, B. H., Hopfner, K. P., Holzmann, K., Russo, R., Esposito, M. R., Spano, D., De Falco, L., Heinrich, K., Joggerst, B., Rojewski, M. T., Perrotta, S., Denecke, J., Pannicke, U., Delaunay, J., Pepperkok, R., and Heimpel, H. (2009) Mutations affecting the secretory COPII coat component SEC23B cause congenital dyserythropoietic anemia type II. *Nat. Genet.* 41, 936–940.
- (20) Wansleeben, C., Feitsma, H., Montcouquiol, M., Kroon, C., Cuppen, E., and Meijlink, F. (2010) Planar cell polarity defects and defective Vangl2 trafficking in mutants for the COPII gene Sec24b. *Development* 137, 1067–1073.
- (21) Fromme, J. C., Ravazzola, M., Hamamoto, S., Al-Balwi, M., Eyaid, W., Boyadjiev, S. A., Cosson, P., Schekman, R., and Orci, L. (2007) The genetic basis of a craniofacial disease provides insight into COPII coat assembly. *Dev. Cell* 13, 623–634.
- (22) Garbes, L., Kim, K., Riess, A., Hoyer-Kuhn, H., Beleggia, F., Bevon, A., Kim, M. J., Huh, Y. H., Kweon, H. S., Savarirayan, R., Amor, D., Kakadia, P. M., Lindig, T., Kagan, K. O., Becker, J., Boyadjiev, S. A., Wollnik, B., Semler, O., Bohlander, S. K., Kim, J., and Netzer, C. (2015) Mutations in SEC24D, encoding a component of the COPII machinery, cause a syndromic form of osteogenesis imperfecta. *Am. J. Hum. Genet.* 96, 432–439.
- (23) Moosa, S., Chung, B. H., Tung, J. Y., Altmuller, J., Thiele, H., Nurnberg, P., Netzer, C., Nishimura, G., and Wollnik, B. (2016) Mutations in SEC24D cause autosomal recessive osteogenesis imperfecta. *Clin. Genet.* 89, 517.
- (24) Oz-Levi, D., Ben-Zeev, B., Ruzzo, E. K., Hitomi, Y., Gelman, A., Pelak, K., Anikster, Y., Reznik-Wolf, H., Bar-Joseph, I., Olender, T., Alkelai, A., Weiss, M., Ben-Asher, E., Ge, D., Shianna, K. V., Elazar, Z., Goldstein, D. B., Pras, E., and Lancet, D. (2012) Mutation in TECPR2 reveals a role for autophagy in hereditary spastic paraparesis. *Am. J. Hum. Genet.* 91, 1065–1072.
- (25) Stadel, D., Millarte, V., Tillmann, K. D., Huber, J., Tamin-Yecheskel, B. C., Akutsu, M., Demishtein, A., Ben-Zeev, B., Anikster, Y., Perez, F., Dotsch, V., Elazar, Z., Rogov, V., Farhan, H., and Behrends, C. (2015) TECPR2 Cooperates with LC3C to Regulate COPII-Dependent ER Export. *Mol. Cell* 60, 89–104.
- (26) Boyadjiev, S. A., Kim, S. D., Hata, A., Haldeman-Englert, C., Zackai, E. H., Naydenov, C., Hamamoto, S., Schekman, R. W., and Kim, J. (2011) Cranio-lenticulo-sutural dysplasia associated with defects in collagen secretion. *Clin. Genet.* 80, 169–176.
- (27) Melville, D. B., Montero-Balaguer, M., Levic, D. S., Bradley, K., Smith, J. R., Hatzopoulos, A. K., and Knapik, E. W. (2011) The feelgood mutation in zebrafish dysregulates COPII-dependent secretion of select extracellular matrix proteins in skeletal morphogenesis. *Dis. Models & Mech.* 4, 763–776.
- (28) Sarmah, S., Barrallo-Gimeno, A., Melville, D. B., Topczewski, J., Solnica-Krezel, L., and Knapik, E. W. (2010) Sec24D-dependent transport of extracellular matrix proteins is required for zebrafish skeletal morphogenesis. *PLoS One* 5, e10367.
- (29) Malhotra, V., and Erlmann, P. (2015) The pathway of collagen secretion. *Annu. Rev. Cell Dev. Biol.* 31, 109–124.
- (30) Ohisa, S., Inohaya, K., Takano, Y., and Kudo, A. (2010) sec24d encoding a component of COPII is essential for vertebra formation, revealed by the analysis of the medaka mutant, vbi. *Dev. Biol.* 342, 85–95.
- (31) Harding, H. P., Zhang, Y., and Ron, D. (1999) Protein translation and folding are coupled by an endoplasmic-reticulum-resident kinase. *Nature* 397, 271–274.
- (32) Travers, K. J., Patil, C. K., Wodicka, L., Lockhart, D. J., Weissman, J. S., and Walter, P. (2000) Functional and genomic analyses reveal an essential coordination between the unfolded protein response and ER-associated degradation. *Cell* 101, 249–258.
- (33) Shaffer, A. L., Shapiro-Shelef, M., Iwakoshi, N. N., Lee, A. H., Qian, S. B., Zhao, H., Yu, X., Yang, L., Tan, B. K., Rosenwald, A., Hurt, E. M., Petroulakis, E., Sonenberg, N., Yewdell, J. W., Calame, K., Glimcher, L. H., and Staudt, L. M. (2004) XBP1, downstream of Blimp-1, expands the secretory apparatus and other organelles, and increases protein synthesis in plasma cell differentiation. *Immunity* 21, 81–93.
- (34) Hetz, C., Chevet, E., and Harding, H. P. (2013) Targeting the unfolded protein response in disease. *Nat. Rev. Drug Discovery* 12, 703–719.
- (35) Wang, S., and Kaufman, R. J. (2012) The impact of the unfolded protein response on human disease. *J. Cell Biol.* 197, 857–867.
- (36) Farhan, H., Weiss, M., Tani, K., Kaufman, R. J., and Hauri, H. P. (2008) Adaptation of endoplasmic reticulum exit sites to acute and chronic increases in cargo load. *EMBO J.* 27, 2043–2054.
- (37) Ron, D., and Walter, P. (2007) Signal integration in the endoplasmic reticulum unfolded protein response. *Nat. Rev. Mol. Cell Biol.* 8, 519–529.
- (38) Lord, C., Bhandari, D., Menon, S., Ghassemian, M., Nycz, D., Hay, J., Ghosh, P., and Ferro-Novick, S. (2011) Sequential interactions with Sec23 control the direction of vesicle traffic. *Nature* 473, 181–186.
- (39) Bhandari, D., Zhang, J., Menon, S., Lord, C., Chen, S., Helm, J. R., Thorsen, K., Corbett, K. D., Hay, J. C., and Ferro-Novick, S. (2013) Sit4p/PP6 regulates ER-to-Golgi traffic by controlling the dephosphorylation of COPII coat subunits. *Molecular biology of the cell* 24, 2727–2738.
- (40) Farhan, H., Wendeler, M. W., Mitrovic, S., Fava, E., Silberberg, Y., Sharan, R., Zerial, M., and Hauri, H. P. (2010) MAPK signaling to the early secretory pathway revealed by kinase/phosphatase functional screening. *J. Cell Biol.* 189, 997–1011.
- (41) Zacharogianni, M., Kondylis, V., Tang, Y., Farhan, H., Xanthakis, D., Fuchs, F., Boutros, M., and Rabouille, C. (2011) ERK7 is a negative regulator of protein secretion in response to amino-acid

starvation by modulating Sec16 membrane association. *EMBO J.* 30, 3684–3700.

(42) Sharpe, L. J., Luu, W., and Brown, A. J. (2011) Akt phosphorylates Sec24: new clues into the regulation of ER-to-Golgi trafficking. *Traffic* 12, 19–27.

(43) Palmer, K. J., Konkel, J. E., and Stephens, D. J. (2005) PCTAIRE protein kinases interact directly with the COPII complex and modulate secretory cargo transport. *J. Cell Biol.* 118, 3839–3847.

(44) Koreishi, M., Yu, S., Oda, M., Honjo, Y., and Satoh, A. (2013) CK2 phosphorylates Sec31 and regulates ER-To-Golgi trafficking. *PLoS One* 8, e54382.

(45) Cohen, M., Stutz, F., Belgareh, N., Haguenaer-Tsapis, R., and Dargemont, C. (2003) Ubp3 requires a cofactor, Bre5, to specifically de-ubiquitinate the COPII protein, Sec23. *Nat. Cell Biol.* 5, 661–667.

(46) Jin, L., Pahuja, K. B., Wickliffe, K. E., Gorur, A., Baumgartel, C., Schekman, R., and Rape, M. (2012) Ubiquitin-dependent regulation of COPII coat size and function. *Nature* 482, 495–500.

(47) McGourty, C. A., Akopian, D., Walsh, C., Gorur, A., Werner, A., Schekman, R., Bautista, D., and Rape, M. (2016) Regulation of the CUL3 Ubiquitin Ligase by a Calcium-Dependent Co-adaptor. *Cell* 167, 525–538.

(48) Boyce, M., Carrico, I. S., Ganguli, A. S., Yu, S. H., Hangauer, M. J., Hubbard, S. C., Kohler, J. J., and Bertozzi, C. R. (2011) Metabolic cross-talk allows labeling of O-linked beta-N-acetylglucosamine-modified proteins via the N-acetylgalactosamine salvage pathway. *Proc. Natl. Acad. Sci. U. S. A.* 108, 3141–3146.

(49) Zachara, N. E., Molina, H., Wong, K. Y., Pandey, A., and Hart, G. W. (2011) The dynamic stress-induced "O-GlcNAc-ome" highlights functions for O-GlcNAc in regulating DNA damage/repair and other cellular pathways. *Amino Acids* 40, 793–808.

(50) Dudognon, P., Maeder-Garavaglia, C., Carpentier, J. L., and Paccard, J. P. (2004) Regulation of a COPII component by cytosolic O-glycosylation during mitosis. *FEBS Lett.* 561, 44–50.

(51) Teo, C. F., Ingale, S., Wolfert, M. A., Elsayed, G. A., Not, L. G., Chatham, J. C., Wells, L., and Boons, G. J. (2010) Glycopeptide-specific monoclonal antibodies suggest new roles for O-GlcNAc. *Nat. Chem. Biol.* 6, 338–343.

(52) Lee, A., Miller, D., Henry, R., Paruchuri, V. D., O'Meally, R. N., Boronina, T., Cole, R. N., and Zachara, N. E. (2016) Combined Antibody/Lectin Enrichment Identifies Extensive Changes in the O-GlcNAc Sub-proteome upon Oxidative Stress. *J. Proteome Res.* 15, 4318–4336.

(53) Hanover, J. A., Krause, M. W., and Love, D. C. (2010) The hexosamine signaling pathway: O-GlcNAc cycling in feast or famine. *Biochim. Biophys. Acta, Gen. Subj.* 1800, 80–95.

(54) Hart, G. W., Slawson, C., Ramirez-Correa, G., and Lagerlof, O. (2011) Cross talk between O-GlcNAcylation and phosphorylation: roles in signaling, transcription, and chronic disease. *Annu. Rev. Biochem.* 80, 825–858.

(55) Bond, M. R., and Hanover, J. A. (2015) A little sugar goes a long way: the cell biology of O-GlcNAc. *J. Cell Biol.* 208, 869–880.

(56) Hart, G. W. (2014) Three Decades of Research on O-GlcNAcylation - A Major Nutrient Sensor That Regulates Signaling, Transcription and Cellular Metabolism. *Front. Endocrinol.* 5, 183.

(57) Shafi, R., Iyer, S. P., Ellies, L. G., O'Donnell, N., Marek, K. W., Chui, D., Hart, G. W., and Marth, J. D. (2000) The O-GlcNAc transferase gene resides on the X chromosome and is essential for embryonic stem cell viability and mouse ontogeny. *Proc. Natl. Acad. Sci. U. S. A.* 97, 5735–5739.

(58) Keembiyehetty, C., Love, D. C., Harwood, K. R., Gavrilo, O., Comly, M. E., and Hanover, J. A. (2015) Conditional knockout reveals a requirement for O-GlcNAcase in metabolic homeostasis. *J. Biol. Chem.* 290, 7097–7113.

(59) Gloster, T. M., Zandberg, W. F., Heinonen, J. E., Shen, D. L., Deng, L., and Vocadlo, D. J. (2011) Hijacking a biosynthetic pathway yields a glycosyltransferase inhibitor within cells. *Nat. Chem. Biol.* 7, 174–181.

(60) Yu, S. H., Boyce, M., Wands, A. M., Bond, M. R., Bertozzi, C. R., and Kohler, J. J. (2012) Metabolic labeling enables selective

photocrosslinking of O-GlcNAc-modified proteins to their binding partners. *Proc. Natl. Acad. Sci. U. S. A.* 109, 4834–4839.

(61) Yuzwa, S. A., Macauley, M. S., Heinonen, J. E., Shan, X., Dennis, R. J., He, Y., Whitworth, G. E., Stubbs, K. A., McEachern, E. J., Davies, G. J., and Vocadlo, D. J. (2008) A potent mechanism-inspired O-GlcNAcase inhibitor that blocks phosphorylation of tau in vivo. *Nat. Chem. Biol.* 4, 483–490.

(62) Sambrook, J., Fritsch, E. F., and Maniatis, T. (1989) *Molecular Cloning, A Laboratory Manual*, 2nd ed., Cold Spring Harbor Laboratory Press, Plainview, NY.

(63) Schindelin, J., Arganda-Carreras, I., Frise, E., Kaynig, V., Longair, M., Pietzsch, T., Preibisch, S., Rueden, C., Saalfeld, S., Schmid, B., Tinevez, J. Y., White, D. J., Hartenstein, V., Eliceiri, K., Tomancak, P., and Cardona, A. (2012) Fiji: an open-source platform for biological-image analysis. *Nat. Methods* 9, 676–682.

(64) Ran, F. A., Hsu, P. D., Wright, J., Agarwala, V., Scott, D. A., and Zhang, F. (2013) Genome engineering using the CRISPR-Cas9 system. *Nat. Protoc.* 8, 2281–2308.

(65) Sadelain, M., Papapetrou, E. P., and Bushman, F. D. (2011) Safe harbours for the integration of new DNA in the human genome. *Nat. Rev. Cancer* 12, 51–58.

(66) Cutrona, M. B., Beznoussenko, G. V., Fusella, A., Martella, O., Moral, P., and Mironov, A. A. (2013) Silencing of mammalian Sar1 isoforms reveals COPII-independent protein sorting and transport. *Traffic* 14, 691–708.

(67) Dale, R. M., and Topczewski, J. (2011) Identification of an evolutionarily conserved regulatory element of the zebrafish col2a1a gene. *Dev. Biol.* 357, 518–531.

(68) Schindelin, J., Rueden, C. T., Hiner, M. C., and Eliceiri, K. W. (2015) The ImageJ ecosystem: An open platform for biomedical image analysis. *Mol. Reprod. Dev.* 82, 518–529.

(69) Bi, X., Corpina, R. A., and Goldberg, J. (2002) Structure of the Sec23/24-Sar1 pre-budding complex of the COPII vesicle coat. *Nature* 419, 271–277.

(70) Zanetti, G., Prinz, S., Daum, S., Meister, A., Schekman, R., Bacia, K., and Briggs, J. A. (2013) The structure of the COPII transport-vesicle coat assembled on membranes. *eLife* 2, e00951.

(71) Fath, S., Mancias, J. D., Bi, X., and Goldberg, J. (2007) Structure and organization of coat proteins in the COPII cage. *Cell* 129, 1325–1336.

(72) Stagg, S. M., LaPointe, P., Razvi, A., Gurkan, C., Potter, C. S., Carragher, B., and Balch, W. E. (2008) Structural basis for cargo regulation of COPII coat assembly. *Cell* 134, 474–484.

(73) Bhattacharya, N., O'Donnell, J., and Stagg, S. M. (2012) The structure of the Sec13/31 COPII cage bound to Sec23. *J. Mol. Biol.* 420, 324–334.

(74) Bi, X., Mancias, J. D., and Goldberg, J. (2007) Insights into COPII coat nucleation from the structure of Sec23.Sar1 complexed with the active fragment of Sec31. *Dev. Cell* 13, 635–645.

(75) Elsayed, L. E., Mohammed, I. N., Hamed, A. A., Elseed, M. A., Johnson, A., Mairey, M., Mohamed, H. E., Idris, M. N., Salih, M. A., El-Sadig, S. M., Koko, M. E., Mohamed, A. Y., Raymond, L., Coutelier, M., Darios, F., Siddig, R. A., Ahmed, A. K., Babai, A. M., Malik, H. M., Omer, Z. M., Mohamed, E. O., Eltahir, H. B., Magboul, N. A., Bushara, E. E., Elnour, A., Rahim, S. M., Alattaya, A., Elbashir, M. I., Ibrahim, M. E., Durr, A., Audhya, A., Brice, A., Ahmed, A. E., and Stevanin, G. (2016) Hereditary spastic paraplegias: identification of a novel SPG57 variant affecting TFG oligomerization and description of HSP subtypes in Sudan. *Eur. J. Hum. Genet.* 25, 100–110.

(76) Witte, K., Schuh, A. L., Hegermann, J., Sarkeshik, A., Mayers, J. R., Schwarze, K., Yates, J. R., III, Eimer, S., and Audhya, A. (2011) TFG-1 function in protein secretion and oncogenesis. *Nat. Cell Biol.* 13, 550–558.

(77) Johnson, A., Bhattacharya, N., Hanna, M., Pennington, J. G., Schuh, A. L., Wang, L., Otegui, M. S., Stagg, S. M., and Audhya, A. (2015) TFG clusters COPII-coated transport carriers and promotes early secretory pathway organization. *EMBO J.* 34, 811–827.

(78) Bard, F., Casano, L., Mallabiabarrena, A., Wallace, E., Saito, K., Kitayama, H., Guizzunti, G., Hu, Y., Wendler, F., Dasgupta, R.,

Perrimon, N., and Malhotra, V. (2006) Functional genomics reveals genes involved in protein secretion and Golgi organization. *Nature* 439, 604–607.

(79) Presley, J. F., Cole, N. B., Schroer, T. A., Hirschberg, K., Zaal, K. J., and Lippincott-Schwartz, J. (1997) ER-to-Golgi transport visualized in living cells. *Nature* 389, 81–85.

(80) Scales, S. J., Pepperkok, R., and Kreis, T. E. (1997) Visualization of ER-to-Golgi transport in living cells reveals a sequential mode of action for COPII and COPI. *Cell* 90, 1137–1148.

(81) Reid, D. W., Chen, Q., Tay, A. S., Shenolikar, S., and Nicchitta, C. V. (2014) The unfolded protein response triggers selective mRNA release from the endoplasmic reticulum. *Cell* 158, 1362–1374.

(82) Mondoux, M. A., Love, D. C., Ghosh, S. K., Fukushige, T., Bond, M., Weerasinghe, G. R., Hanover, J. A., and Krause, M. W. (2011) O-linked-N-acetylglucosamine cycling and insulin signaling are required for the glucose stress response in *Caenorhabditis elegans*. *Genetics* 188, 369–382.

(83) Bond, M. R., and Hanover, J. A. (2013) O-GlcNAc cycling: a link between metabolism and chronic disease. *Annu. Rev. Nutr.* 33, 205–229.

(84) Barlowe, C., and Helenius, A. (2016) Cargo Capture and Bulk Flow in the Early Secretory Pathway. *Annu. Rev. Cell Dev. Biol.* 32, 197–222.

(85) Malhotra, V., Erlmann, P., and Nogueira, C. (2015) Procollagen export from the endoplasmic reticulum. *Biochem. Soc. Trans.* 43, 104–107.

(86) Vincourt, J. B., Etienne, S., Cottet, J., Delaunay, C., Malanda, C. B., Lionneton, F., Sirveaux, F., Netter, P., Plenat, F., Mainard, D., Vignaud, J. M., and Magdalou, J. (2010) C-propeptides of procollagens I alpha 1 and II that differentially accumulate in enchondromas versus chondrosarcomas regulate tumor cell survival and migration. *Cancer Res.* 70, 4739–4748.

(87) Aigner, T. (2002) Towards a new understanding and classification of chondrogenic neoplasias of the skeleton—biochemistry and cell biology of chondrosarcoma and its variants. *Virchows Arch.* 441, 219–230.

(88) Kim, S. D., Pahuja, K. B., Ravazzola, M., Yoon, J., Boyadjiev, S. A., Hammamoto, S., Schekman, R., Orci, L., and Kim, J. (2012) The [corrected] SEC23-SEC31 [corrected] interface plays critical role for export of procollagen from the endoplasmic reticulum. *J. Biol. Chem.* 287, 10134–10144.

(89) Melville, D. B., and Knapik, E. W. (2011) Traffic jams in fish bones: ER-to-Golgi protein transport during zebrafish development. *Cell Adh Migr* 5, 114–118.

(90) Unlu, G., Levic, D. S., Melville, D. B., and Knapik, E. W. (2014) Trafficking mechanisms of extracellular matrix macromolecules: insights from vertebrate development and human diseases. *Int. J. Biochem. Cell Biol.* 47, 57–67.

(91) Matsuoka, K., Orci, L., Amherdt, M., Bednarek, S. Y., Hamamoto, S., Schekman, R., and Yeung, T. (1998) COPII-coated vesicle formation reconstituted with purified coat proteins and chemically defined liposomes. *Cell* 93, 263–275.

(92) Kettenbach, A. N., Schweppe, D. K., Faherty, B. K., Pechenick, D., Pletnev, A. A., and Gerber, S. A. (2011) Quantitative phosphoproteomics identifies substrates and functional modules of Aurora and Polo-like kinase activities in mitotic cells. *Sci. Signaling* 4, rs5.

(93) Chen, X. W., Wang, H., Bajaj, K., Zhang, P., Meng, Z. X., Ma, D., Bai, Y., Liu, H. H., Adams, E., Baines, A., Yu, G., Sartor, M. A., Zhang, B., Yi, Z., Lin, J., Young, S. G., Schekman, R., and Ginsburg, D. (2013) SEC24A deficiency lowers plasma cholesterol through reduced PCSK9 secretion. *eLife* 2, e00444.

(94) Adams, E. J., Chen, X. W., O'Shea, K. S., and Ginsburg, D. (2014) Mammalian COPII coat component SEC24C is required for embryonic development in mice. *J. Biol. Chem.* 289, 20858–20870.

(95) Baines, A. C., Adams, E. J., Zhang, B., and Ginsburg, D. (2013) Disruption of the *Sec24d* gene results in early embryonic lethality in the mouse. *PLoS One* 8, e61114.

(96) Khoriaty, R., Everett, L., Chase, J., Zhu, G., Hoenerhoff, M., McKnight, B., Vasievich, M. P., Zhang, B., Tomberg, K., Williams, J., Maillard, I., and Ginsburg, D. (2016) Pancreatic SEC23B deficiency is sufficient to explain the perinatal lethality of germline SEC23B deficiency in mice. *Sci. Rep.* 6, 27802.

(97) Khoriaty, R., Vasievich, M. P., Jones, M., Everett, L., Chase, J., Tao, J., Siemieniak, D., Zhang, B., Maillard, I., and Ginsburg, D. (2014) Absence of a red blood cell phenotype in mice with hematopoietic deficiency of SEC23B. *Mol. Cell. Biol.* 34, 3721–3734.

(98) Tao, J., Zhu, M., Wang, H., Afelik, S., Vasievich, M. P., Chen, X. W., Zhu, G., Jensen, J., Ginsburg, D., and Zhang, B. (2012) SEC23B is required for the maintenance of murine professional secretory tissues. *Proc. Natl. Acad. Sci. U. S. A.* 109, E2001–2009.

(99) Zhu, M., Tao, J., Vasievich, M. P., Wei, W., Zhu, G., Khoriaty, R. N., and Zhang, B. (2015) Neural tube opening and abnormal extraembryonic membrane development in SEC23A deficient mice. *Sci. Rep.* 5, 15471.

(100) Andres-Bergos, J., Tardio, L., Larranaga-Vera, A., Gomez, R., Herrero-Baumont, G., and Largo, R. (2012) The increase in O-linked N-acetylglucosamine protein modification stimulates chondrogenic differentiation both in vitro and in vivo. *J. Biol. Chem.* 287, 33615–33628.

(101) Saito, K., Yamashiro, K., Ichikawa, Y., Erlmann, P., Kontani, K., Malhotra, V., and Katada, T. (2011) cTAGE5 mediates collagen secretion through interaction with TANGO1 at endoplasmic reticulum exit sites. *Molecular biology of the cell* 22, 2301–2308.

■ NOTE ADDED AFTER ASAP PUBLICATION

This article was published ASAP on December 15, 2017. Panel C of Figure 4 was missing. The figure has been corrected and reposted on December 18, 2017.